

Influence of openings on two-way bending capacity of unreinforced masonry walls

Chang, L.; Rots, Jan G.; Esposito, Rita

DOI

[10.1016/j.jobe.2022.104222](https://doi.org/10.1016/j.jobe.2022.104222)

Publication date

2022

Document Version

Final published version

Published in

Journal of Building Engineering

Citation (APA)

Chang, L., Rots, J. G., & Esposito, R. (2022). Influence of openings on two-way bending capacity of unreinforced masonry walls. *Journal of Building Engineering*, 51, Article 104222. <https://doi.org/10.1016/j.jobe.2022.104222>

Important note

To cite this publication, please use the final published version (if applicable). Please check the document version above.

Copyright

Other than for strictly personal use, it is not permitted to download, forward or distribute the text or part of it, without the consent of the author(s) and/or copyright holder(s), unless the work is under an open content license such as Creative Commons.

Takedown policy

Please contact us and provide details if you believe this document breaches copyrights. We will remove access to the work immediately and investigate your claim.



Influence of openings on two-way bending capacity of unreinforced masonry walls

Lang-Zi Chang (常浪子)^{*}, Jan G. Rots, Rita Esposito

Faculty of Civil Engineering and Geosciences, Delft University of Technology, Stevinweg 1, 2628 CN, Delft, the Netherlands

ARTICLE INFO

Keywords:

Unreinforced masonry
Two-way bending
Opening
3D simplified brick-to-brick modelling
Standard

ABSTRACT

Perforated unreinforced masonry (URM) walls in out-of-plane (OOP) two-way bending are commonly encountered in natural hazard investigations. However, related research is rather limited. This study focuses on the influence of openings on the two-way bending capacity of URM walls. An experimental database about the perforated URM walls in OOP two-way bending was created. A brief review of the experimental results show that the arrangement of the opening area can significantly affect the two-way bending capacity of walls (defined as the peak pressure on the wall net area): when the opening area is non-covered and non-loaded, the two-way bending capacity of the perforated wall is higher than that of its solid counterpart; when the opening area is covered with timber or glass plates loaded as the rest of the wall, the two-way bending capacity of the perforated wall is lower than that of the corresponding solid wall. These observations from the experiments were confirmed by an analytical estimation using the Yield Line Method (YLM). Next, to study the influence of openings on the two-way bending capacity, a numerical study has been carried out by employing the 3D simplified brick-to-brick modelling approach. The results of calibration and validation show that this modelling approach can precisely predict the two-way bending capacity and crack patterns. By applying the validated numerical models, the influence of the arrangement for the opening area from the experimental results and YLM evaluation was confirmed. Further, a parametric study focusing mainly on cases with the opening area non-covered and non-loaded was conducted. The influence of the geometric parameters of openings, namely, the opening size, shape and position was investigated on walls with different aspect ratios. Results show that the two-way bending capacity increases as the opening size or aspect ratio (height to width) increase, but it is insensitive to the opening position. Eventually, based on the numerical results, analytical equations were proposed to account for the influence of the considered parameters on the two-way bending capacity. A comparison with the Australian Standard (AS3700) indicates that the proposed equations incorporate more opening parameters such as opening shape.

1. Introduction

Perforated walls, i.e. walls with openings (windows and doors), are commonly encountered in unreinforced masonry (URM) buildings. In some countries, such as the Netherlands, openings can be relatively large, as shown in Fig. 1. Therefore, the presence of openings can alter the mechanical behaviour of walls to a large degree. Recent research concerning perforated URM walls focuses on

^{*} Corresponding author.

E-mail addresses: L.Chang-2@tudelft.nl (L.-Z. Chang), J.G.Rots@tudelft.nl (J.G. Rots), R.Esposito@tudelft.nl (R. Esposito).

their in-plane performance [1–3]. In contrast, the research on the walls in out-of-plane (OOP) two-way bending, in which at least one lateral edge of a wall is supported in addition to its top and bottom edges, is relatively limited. However, investigations have identified OOP failure of URM walls subjected to natural hazards, such as earthquakes, as one of the most occurring failure mechanisms [4–8]. It is thus of significance to further study the influence of openings on the two-way bending capacity of URM walls.

Research on this topic started from laboratory experiments back in the 1970s. Most of the experimental campaigns applied quasi-static tests using airbags [9–15], while a few others adopted dynamic tests [16,17]. However, the existing experimental database is limited in quantity, and crucial data such as opening size and position is unavailable, especially in early experimental records. Moreover, different experiments adopted different arrangements for the opening area. Some covered the opening area with timber or glass plates and loaded it with uniformly distributed pressure as the rest of the wall, while the others left the opening area empty and non-loaded. This led to contradictory conclusions on the influence of the openings on the two-way bending capacity of the walls. Furthermore, only a few experiments systematically studied the geometric parameters of the opening, namely size, shape and position. Thus, solid conclusions about these parameters cannot be drawn due to the limited number of samples [11,13]. A brief review of the available database elaborating on the experimental details and findings is provided in Section 2.

Numerical modelling, especially nonlinear finite element analysis, has been introduced to study the mechanical behaviour of URM walls in OOP two-way bending. Among various modelling techniques, the 3D simplified brick-to-brick modelling has been proved to be an effective method in studying the solid URM walls, considering that it can well present the wall crack pattern [18–22]. Concerning perforated walls, Nasiri and Liu [23] used 3D simplified brick-to-brick modelling to study the influence of a central window on masonry infills within reinforced concrete frameworks. However, according to the authors' knowledge, there is no research applying this modelling technique to systematically study the influence of openings on the two-way bending capacity of URM walls.

The insufficient research regarding perforated URM walls in OOP two-way bending results in incomplete analytical formulations in current building standards. In some major standards, such as Eurocode 6 – Design of Masonry Structures [24], large openings that potentially influence the wall behaviour are required to be evaluated using additional analysis tools. By contrast, the Australian Standard – Masonry Structures (AS3700) [25] takes the opening length and horizontal position into account. Within limited ranges, the two-way bending capacity of the perforated walls is reported to decrease as the opening length increases, or as the opening moves from the wall centre towards the lateral edges [26]. However, the predictions by AS3700 can be contradictory with some experimental results and can overly underestimate the two-way bending capacity of the perforated walls. Besides, the opening aspect ratio is not considered in AS3700. This poses questions regarding the accuracy of the related analytical formulations in AS3700 and calls for further study on perforated URM walls in OOP two-way bending.

This study focuses on the influence of openings on the two-way bending capacity of URM walls. The influence of the arrangement of the opening and the opening geometric parameters, i.e. size, shape and position are specifically explored. First, available experimental records were collected and analysed to provide a brief review of the observations and limitations of existing experimental campaigns (Section 2). A preliminary evaluation of the influence of openings by the Yield Line Method was conducted in Section 3. Then, 3D simplified brick-to-brick finite element models were calibrated and validated based on the experimental campaign carried out by Griffith and Vaculik [14] (Section 4). The influence of the arrangement of the opening area was studied with various virtual settings in Section 5. Further, a parametric study was carried out to evaluate the influence of the opening geometric parameters, such as type (window or door), size, shape and position on both long and short walls (Section 6). Eventually, proposed equations based on the numerical results were proposed and compared with AS3700 (Section 7).

2. A brief review of the available experimental database

As introduced in Section 1, experiments on perforated URM walls in OOP two-way bending have been carried out from the 1970s onwards. A database dating from 1977 is collected and presented in Table 1. The database consists of 9 testing campaigns and 19 groups of samples. Each group contains at most one solid wall as a reference and at least one perforated wall having identical testing configurations as the former. In the majority of the cases, quasi-static tests were performed by applying a uniformly distributed pressure on the wall surface with airbags (Fig. 2a). In a few cases, dynamic loads were applied using shake-tables. Besides, two arrangements of the opening area can be distinguished. In the first case, the opening area is non-covered and non-loaded, as shown in



Fig. 1. Unreinforced masonry walls with large openings in the Netherlands.

Table 1
Database of experiments on the influence of openings on the two-way bending capacity of URM walls (1977–2019).

Testing campaign	Groups	Testing method ^a	Unit type	Boundary conditions ^b	Wall dimensions $H_w \times L_w \times t_w$ (mm)	Number of samples	Serial number		Opening area (A opening / A gross)	Opening eccentricity	Opening area covered and loaded?	The ratio of two-way bending capacity between the perforated wall (s) and the solid wall
							Solid wall	Walls with openings				
BCRA (1977–1986)	1	Mon.	Clay Brick	U	2600 × 2700 × 100	5	1135	1142, 1143, 1155, 1175	11% (2), 38% (2)	Centric	Unknown	0.68–0.98
	2	Mon.	Clay Brick	U	2600 × 3700 × 100	4	None	1196, 1197, 1200, 1204	8% (3), 28% (1)	Centric	Unknown	Unknown
	3	Mon.	Clay Brick	U	2600 × 5500 × 100	7	None	1128, 1129, 1131, 1132, 1134, 1139, 1141	6% (4), 19% (3)	Centric	Unknown	Unknown
Tapp and Southcombe (1985 & 1988) ^c	4	Mon.	Clay Brick	U	2417 × 4840 × 102.5	3	None	Panel 1, 2, 3	10%, 14%, 18%	Centric	Yes ^d	Unknown
	5	Mon.	Clay Brick	U	2465 × 4715 × 102.5	6	ART01	ART02 - 06	14% (3), 15% (2)	Centric (4); eccentric (1)	Yes ^d	0.57–0.63
Chong (1993)	6	Mon.	Clay Brick	U	2475 × 5615 × 102.5	4	SB01	SB02, 03, 04	18%, 11%, 13%	Centric	Yes	0.76–0.85
	7	Mon.	Clay Brick	U	2450 × 2900 × 102.5	2	SB06	SB07	12%	Centric	Yes	0.73
	8	Mon.	Concrete Block	U	2475 × 5615 × 100	2	DC01	DC02	18%	Centric	Yes	0.66
de Vekey et al. (1996) ^e	9	Mon.	Clay Brick	C	2475 × 2700 × 102.5	4	HW01	HW02 - 04	4%, 8%, 7%	Centric	Yes	0.76–1
	10	Mon.	Brick	O	2600 × 5500 × (Unknown)	3	1a-control	1a(i), 1a (ii)	27% (2)	Centric	Yes	0.77, 1.77
	11	Mon.	Block	O	2600 × 5500 × (Unknown)	3	1b-control	1b(i), 1b (ii)	27% (2)	Centric	Yes	0.93, 1.47
Chen (2002) ^f	12	Mon.	Brick	C	2600 × 5500 × (Unknown)	2	2-control	2a (ii)	28%	Centric	Yes	1
	13	Mon.	Unknown	O	2800 × 5800 × (Unknown)	8	1	2–8	9%–27%	Centric (5); eccentric (2)	Yes	0.68–0.89

(continued on next page)

Table 1 (continued)

Testing campaign	Groups	Testing method ^a	Unit type	Boundary conditions ^b	Wall dimensions $H_w \times L_w \times t_w$ (mm)	Number of samples	Serial number		Opening area (A _{opening} / A _{gross})	Opening eccentricity	Opening area covered and loaded?	The ratio of two-way bending capacity between the perforated wall (s) and the solid wall
							Solid wall	Walls with openings				
Griffith and Vaculik (2007)	14	Mon./Cyc.	Clay Brick	O	2494 × 4200 × 110	2	Wall 1	Wall 3	12%	Eccentric	No	1.06
	15	Mon./Cyc.	Clay Brick	O	2494 × 4200 × 110	2	Wall 2 ^g	Wall 5	12%	Eccentric	No	1.18
Vaculik (2012)	16	Dyn.	Clay Brick	O	1232 × 1840 × 50	2	d1 ^h	d3	13%	Eccentric	No	0.68
	17	Dyn.	Clay Brick	O	1232 × 1840 × 50	2	d2 ^h	d5	13%	Eccentric	No	0.65
Ravenshorst and Messali (2016)	18	Cyc.	Calcium silicate	O	2765 × 3986 × 102	2	TUD_COMP-11	TUD_COMP-12	26%	Eccentric	No	1.49
Graziotti et al. (2019)	19	Dyn.	Calcium silicate	O	2750 × 3980 × 102	2	CS-000-RF	CSW-000-RF	27%	Eccentric	No	0.88
Total	–	–	–	–	–	65	–	–	–	–	–	–

Remarks: a. Mon. = monotonic quasi static test; Cyc. = cyclic quasi-static test; Dyn. = dynamic test; b. U = top free; C = one vertical edge free; O = four-side constrained; c. reported by Chong [11]; d. speculated from information provided in Ref. [11]; e. reported by Edgell and kjaer [31]; f. reported by Baker et al. [32]; g. the bottom edge of Wall 2 was less constrained than other samples, which caused OOP sliding; h. additional constraints were applied to the vertical edges of d1 and d2.

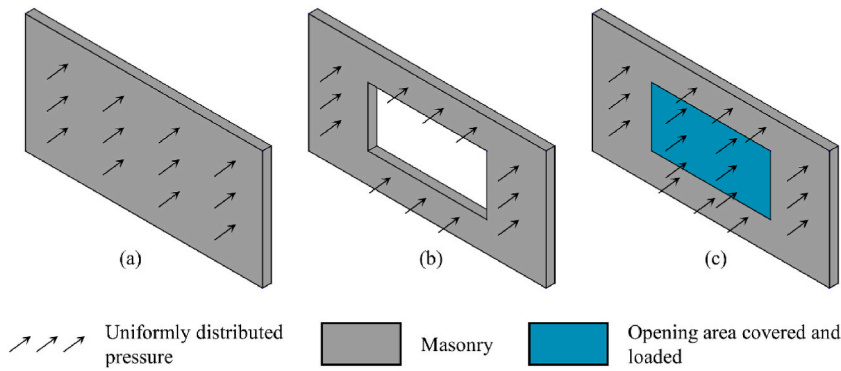


Fig. 2. Schematic diagrams of wall configurations and opening arrangements in the experiments: (a) solid wall; (b) perforated wall with opening area non-covered and non-loaded; (c) perforated wall with the opening area covered with timber or glass plates, and loaded as the rest of the wall.

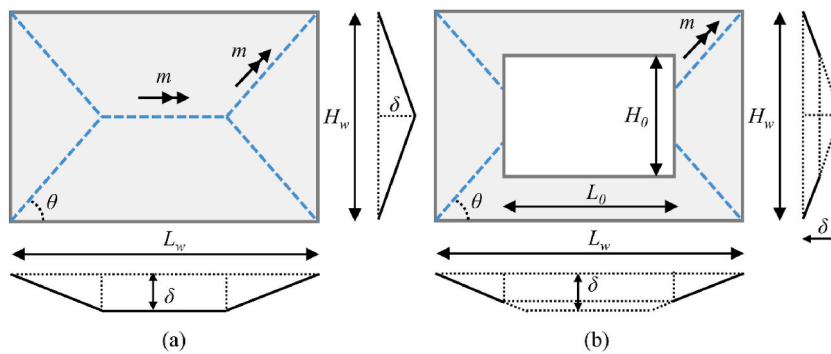


Fig. 3. Yield line patterns: (a) solid wall; (b) perforated wall with a central window.

Fig. 2b; in the second case, the opening area is covered with timber or glass plates and loaded as the rest of the wall, as shown in Fig. 2c. Although the intentions for these different arrangements have not been explained by the researchers, the former arrangement can be considered representative of seismic scenarios, while the latter can be considered representative of wind-loaded scenarios. In this paper, the two-way bending capacity of URM walls is defined as the peak pressure applied to the wall net area. In the case of the opening area covered and loaded, the opening area is included in the wall net area. This definition has the following advantages over defining the wall capacity in terms of the resultant force. First, it follows the conventions of the experiments and current standards such as Eurocode 6 [24] and the Australian Standard [25] and is beneficial for future improvements on the analytical formulations. Second, this definition reflects the most common loading conditions, namely evenly distributed loads caused by wind or earthquake, of URM walls in OOP two-way bending. Third, comparisons of capacity among walls with various dimensions are possible with this definition since it reflects the dissipated fracture energy per wall surface area.

Despite the database being diverse in terms of the testing method, unit type, boundary condition, wall aspect ratio and opening

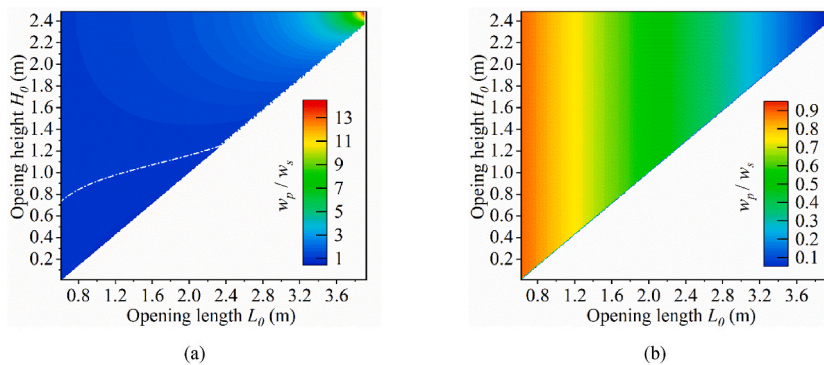


Fig. 4. Normalised two-way bending capacity of the perforated wall to the solid wall based on YLM evaluations in two scenarios: (a) the opening is non-covered and unloaded; (b) the opening is covered and loaded.

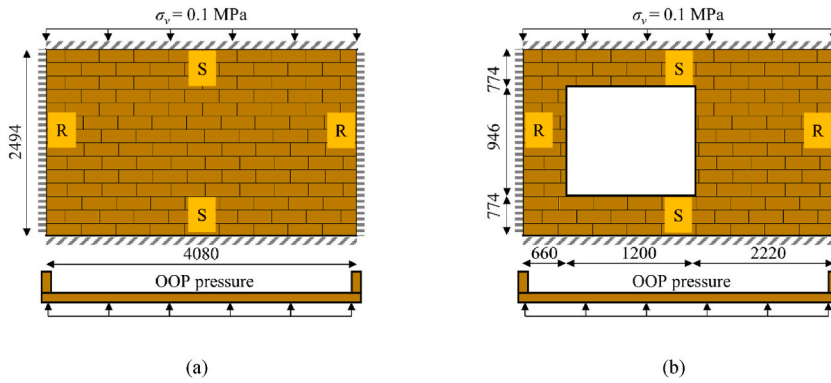


Fig. 5. Sketch of experimental configurations of (a) Wall 1 and (b) Wall 3, respectively. “S” refers to being simply supported; “R” refers to being restrained by return walls. Adapted from Ref. [14].

geometric parameters, the limited number of the perforated walls (only 49 samples) brings difficulty in generalising the experimental observations to a wider application range. Besides, in most of the groups, only one perforated wall can be compared with the solid wall. This can lead to doubts regarding the accuracy of the experimental results since high variability of material properties was widely reported by the testing campaigns. What is more important, different groups draw contradictory conclusions regarding the influence of the openings on the wall capacity. Some experimental results show that the presence of the opening increases the wall capacity, while the others show the opposite. The review of the database shows that these contradictory results can be related to the arrangements of the opening area, namely, whether the openings were covered and loaded. More details of the testing campaigns are elaborated in the following.

The first recorded experiments on perforated URM walls in OOP two-way bending were conducted by British Ceramic Research Association (BCRA) [27,28]. Although 15 perforated walls were tested, only 4 of them can be compared with a referencing solid wall (group 1 in Table 1). Results show that the presence of openings reduces the two-way bending capacity of URM walls. Besides, although walls of different aspect ratios with small ($0.9 \times 0.9 \text{ m}^2$) and large ($2.1 \times 1.3 \text{ m}^2$) openings were tested, the influence of the opening size was unclear (Fig. 5 in Ref. [28]). The arrangements of the openings are ambiguous from available records [27,28]. In Ref. [28], Haseltine and Tutt simply reported that the effect of glazing had been investigated on some walls with openings, and the glazing of the openings had little impact on the wall capacity. Whether the opening area was loaded is unknown. Following BCRA’s testing campaign, Tapp and Southcombe [10,29] conducted two groups of experiments. Results show that the presence of the openings reduces the wall capacity, and the position of the opening has no effect on the wall capacity. The arrangements of the openings are

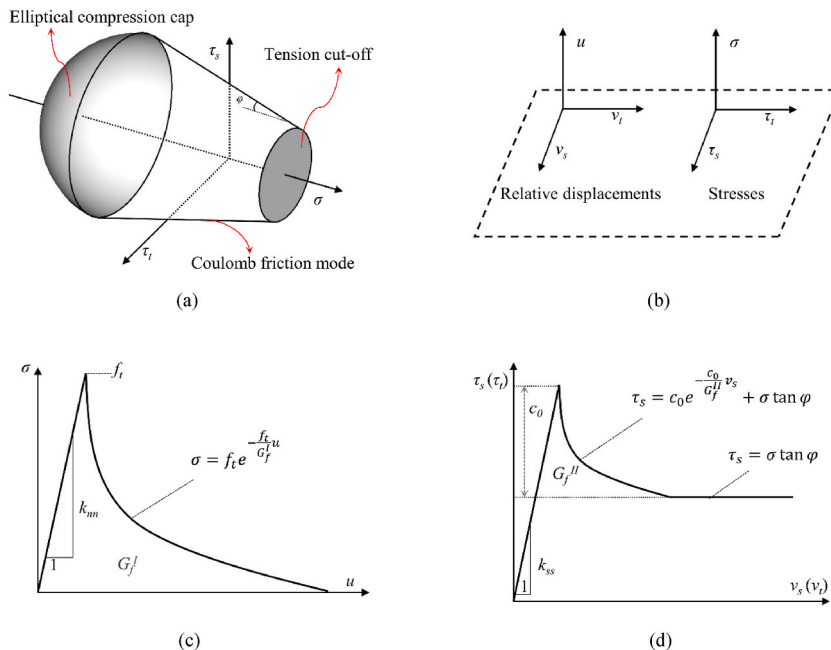


Fig. 6. Combined cracking-shearing-crushing model: (a) multi-surface plasticity model; (b) variables of the 3D interface elements; (c) tensile softening; (d) shear softening.

unknown. However, it can be assumed that since their successor Chong, who covered the opening area with chipboard and loaded it, introduced his testing campaign as “a continuation of the work carried out by Tapp and incorporates a wider range of panels and materials” (page 3 in Ref. [11]), it is reasonable to assume that Tapp and Southcombe applied the same arrangement to the openings. Apart from this, Chong [11] observed a similar effect of the openings on the wall capacity (group 6–9 in Table 1). De Vekey et al. [30] covered and loaded the openings. Based on comparable groups and available results (reported by Edgell and Kjaer [31]), it was found that even though two identical walls with openings were tested, the effect of the openings on the wall capacity can be uncertain (group 10 and 11 in Table 1). Chen [13] tested URM walls with openings of various sizes and positions (group 13 in Table 1, reported by Baker et al. [32]). With the openings covered and loaded, results again show that the presence of the openings reduced the two-way bending capacity. However, a general pattern of the influence of the opening size and position cannot be found.

Different from previous researchers, Griffith and Vaculik [14,33] did not place any frame or covering board, except for the lintel, to the opening area. Therefore, the opening area was non-covered and non-loaded. Counter-intuitively, the two-way bending capacity of the perforated walls is higher than those of the referencing solid walls (groups 14 and 15). Here it should be noted that sample Wall 2 in group 15 was not initially well constrained at the bottom edge as its counterpart, Wall 5, which has an opening. OOP sliding was reported along the bottom edge of Wall 2 [16]. Therefore, the actual influence of the opening in this group is remaining questionable. A similar testing campaign was carried out by Ravenshorst and Messali [15]. The experimental results (group 18) support the observations by Griffith and Vaculik. Vaculik [16] further conducted experiments on half-scale walls subjected to dynamic actions (groups 16 and 17). Though the openings were also non-covered as in his previous experiments, the presence of the openings reduces the wall capacity. However, he also reported that additional timber supports were added to the vertical edges of the solid walls (samples d1 and d2, page 72 in Ref. [16]), which could enhance the fixity of vertical boundary conditions, therefore increasing the wall capacity. Graziotti et al. [17] performed dynamic tests on full-scale URM walls with the opening area left non-covered and non-loaded as well. The reducing effect of the opening on the two-way bending capacity was relatively minor (group 19). A special observation of group 19 is that the crack patterns are quite different between the solid wall (CS-000-RF) and the perforated wall (CSW-000-RF). The former collapsed due to the formation of long vertical line cracks passing through the bricks in the middle and vertical edges of the wall, while the latter only formed local diagonal stepped cracks upon the upper portion of the longer panel beside the opening. This difference is not found in previous testing campaigns in which the solid and perforated walls share the same crack pattern.

Concluding from the experimental database, it is found that, i) the influence of the openings on the wall capacity is related to the arrangements of the openings in the experiments; if the openings were covered and loaded like the masonry part of the wall, the presence of openings could reduce the wall capacity, whereas experiments with openings non-covered and not loaded showed higher wall capacity as compared to a solid wall; ii) the results from the limited number of experimental samples cannot reveal the influence of the geometric parameters of openings on the wall capacity. In an attempt to solve these problems, analytical and numerical methods are adopted in the following sections.

3. Evaluation via Yield Line Method

Section 2 reveals that the arrangements of the opening area can affect the two-way bending capacity of walls. This section aims at evaluating this aspect by applying the Yield Line Method (YLM). The YLM was firstly developed for reinforced concrete slabs and then modified for URM walls by Haseltine et al. [34]. This method was then adopted by the British Masonry Standard [35] that was withdrawn and inherited by Eurocode 6 [24]. However, there has been a longstanding argument that YLM tends to overestimate the two-way bending capacity. This is due to its unrealistic assumptions that moment capacities are reached along all cracks simultaneously, and that the diagonal crack angle is an independent variable [16,36]. Nevertheless, some researchers have shown that YLM can provide acceptable predictions if material properties and boundary conditions were carefully calibrated [28,37,38]. What is more important, YLM is capable of including the openings after minor adaptations [32].

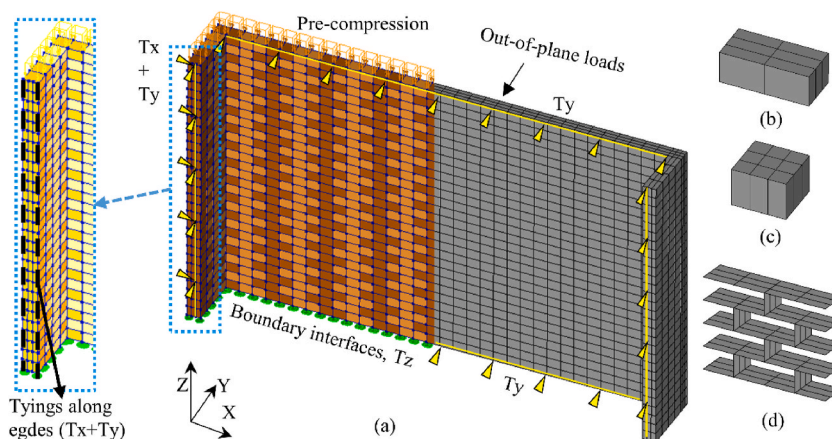


Fig. 7. Modelling settings: (a) geometry, mesh, boundary conditions and loading of the model. Tx, Ty and Tz: d.o.f.s constrained in X, Y and Z direction, respectively; (b) mesh of a complete brick; (c) mesh of a half brick at the intersection; (d) mesh of interface elements.

Table 2
Input parameters of bricks.

Elastic modulus E_b (MPa)	Poisson's ratio ν_b	Density ρ (kg/mm ³)	Tensile strength f_{bt} (MPa)	Fracture energy $G_{f,b}^I$ (N/mm)
52,700	0.16	1900	3.55	0.00355

Table 3
Input parameters of interface elements.

Regime	Parameter	Value
Elastic	Normal stiffness k_m (N/mm ³)	70
	Shear stiffness k_{ss} (ktt) (N/mm ³)	30
	Poisson's ratio ν	0.16
Tension	Tensile strength f_t (MPa)	0.21
	Mode-I fracture energy G_f^I (N/mm)	0.0105
Shearing	Initial cohesion c_0 (MPa)	0.21
	Mode-II fracture energy G_f^{II} (N/mm)	0.105
	Friction angle φ (rad)	0.523
Compression	Compressive strength f_c (MPa)	16

The YLM applied in this section is based on the method for reinforced concrete slabs [39]. The relatively more complicated YLM presented in Refs. [37,38] and Eurocode 6 were not considered here. This aims at comparing the influence of different opening characteristics by YLM via simple examples in a relative sense rather than precisely predicting the wall capacity. The assumptions are, i) moment capacity (m) is equal along all presumed cracks; ii) cracks along boundaries are not considered (simply supported); iii) the diagonal crack angle (θ) is a constant; iv) the OOP load is evenly distributed on the wall; v) the plates divided by yield lines are rigid. Two arrangements of the opening area mentioned in Fig. 2 were considered.

The presumed yield line patterns of a representative solid wall and wall with a central opening are presented in Fig. 3a and b, respectively. In Fig. 3, H_w and L_w are the height and length of the wall, respectively; H_o and L_o are the height and length of the opening, respectively; m is the unit moment capacity of the yield lines; θ is the diagonal crack angle; δ is the virtual OOP displacement. About the solid wall (Fig. 3a), the internal work dissipated along the yield lines is summed as:

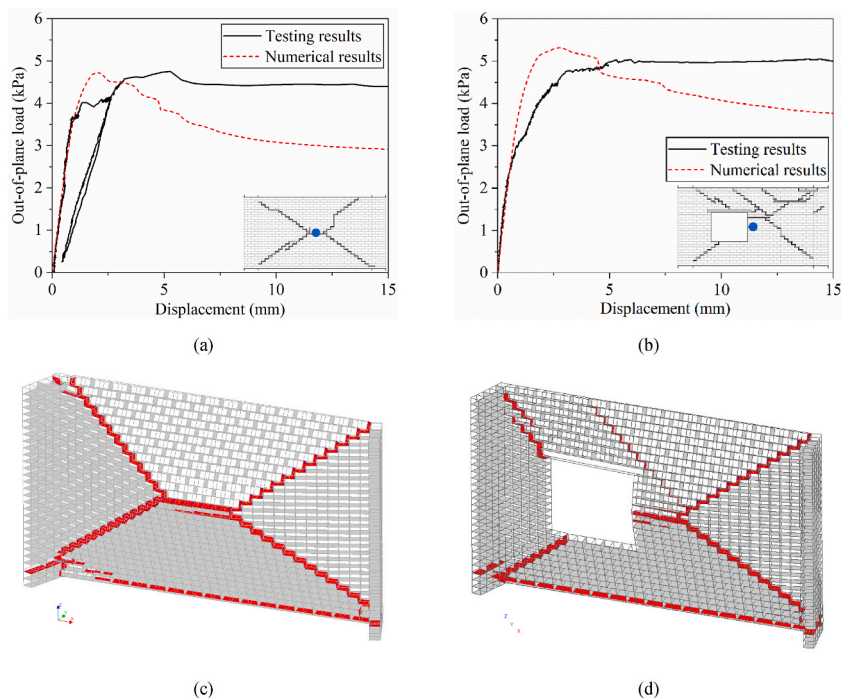


Fig. 8. Calibration and validation based on Wall 1 and Wall 3, respectively: (a) and (b): comparisons of load-displacement curves of Wall 1 and Wall 3, respectively. Testing results are from Ref. [14]; (c) and (d): crack pattern of numerical models of Wall 1 and Wall 3, respectively. Concerning the crack pattern, cracks where f_t reduces to its 1/100 are marked in red. Deformation scaling factor: 20. Positions of recorded displacements are marked with blue dots. (For interpretation of the references to colour in this figure legend, the reader is referred to the Web version of this article.)

Table 4
Comparison in terms of two-way bending capacity between the numerical and experimental results.

Wall	Two-way bending capacity of	
	Experimental results w_{exp} (kPa)	Numerical results w_{num} (kPa)
1	4.76	4.73
3	5.05	5.32
4	3.91	4.65
5	3.59	4.01
6	1.97	2.44
7	8.71	10.36
8	8.52	8.17

Mean Absolute Percentage Error $\left(\frac{1}{n} \sum \frac{|w_{num} - w_{exp}|}{|w_{exp}|}\right)$: 11%.

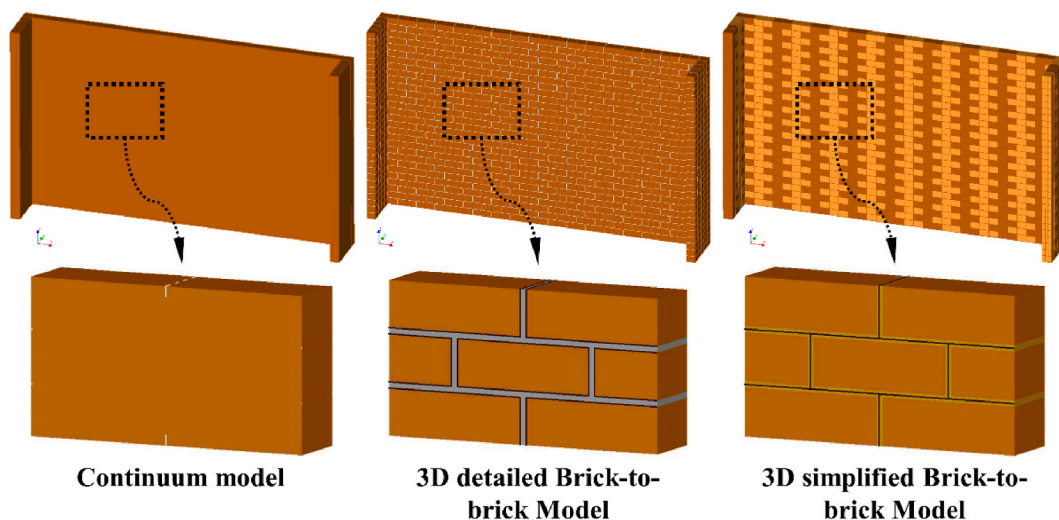


Fig. 10. The geometry of models and zoom-in view of masonry constituents by various approaches.

properties, load-displacement curves under pushover tests and the most realistic boundary conditions among the other comparable perforated and solid walls (Section 2). The sketch of the experimental configurations is shown in Fig. 5. These single-wythe stretch-bond walls were made of $230 \times 110 \times 76 \text{ mm}^3$ clay bricks and 10 mm-thick mortar joints. Both walls were 2494 mm high and 4080 mm long. Wall 1 is solid, while Wall 3 has an opening with dimensions of $946 \times 1200 \text{ mm}^2$ (Fig. 5b). The opening area was non-covered. Both walls were simply supported along the top and bottom edges of the main wall. 480 mm-long return walls were built along the lateral edges of the main wall. C-shape steel channels were used to constrain the lateral edges of the return walls and were simply connected to the supporting frame. On the top of the walls, pre-compression (σ_v) of 0.1 MPa was applied followed by evenly distributed OOP pressure on the outer surface of the masonry, implemented by airbags (Fig. 5). For more details of the experimental configurations, readers are referred to Refs. [14,16].

4.2. Modelling approach and calibrated input parameters

In this study, a 3D simplified brick-to-brick modelling approach was adopted for the simulation of the wall behaviour. With this approach, the bricks are extended in height and length and modelled with solid elements, while the mortar joints are simplified as zero-thickness interfaces. The combined cracking-shearing-crushing model formulated by Lourenco and Rots [40] was applied to the zero-thickness interface elements. The model is based on multi-surface plasticity, comprising a Coulomb friction model combined with a tension cut-off and an elliptical compression cap. The 3D version of this model, enhanced by Van Zijl [41] is presented in Fig. 6a. Variables related to the 3D interface elements are shown in Fig. 6b. A detailed discussion about the modelling process, which includes a detailed analysis of the wall performance together with a sensitivity study on the mesh size and material properties, are reported in a previous study by the authors [22]. For the sake of conciseness, only key aspects of the numerical modelling are introduced in the following sections.

Within the elastic regime, the relation between the normal stress σ and the normal relative displacement u , and that between the shear stress τ_s (τ_t) and the shear relative displacement v_s (v_t), are described as follows:

Table 5
Input parameters for various modelling approaches.

Constitutive models		Input parameters ^a	Modelled constituents of					
			Continuum model		3D detailed model		3D simplified model	
			Masonry	Brick	Mortar	Interface	Brick	Interface
Rotating smear cracking model	Linear material properties	Elastic modulus (N/mm ²)	7080	52,700	442	–	52,700	–
		Poisson's ratio	0.16	0.16	0.16	–	0.16	–
	Tensile behaviour (exponential softening)	Tensile strength (N/mm ²)	0.205	3.55	3.92	–	3.55	–
		Mode-I fracture energy (N/mm)	0.0328	0.355	0.036	–	0.355	–
	Compressive behaviour (parabolic)	Compressive strength (N/mm ²)	16	Elastic	17	–	Elastic	–
Compressive fracture energy (N/mm)		31.5	–	34	–	–	–	
Combined cracking-shearing-crushing model	Linear material properties	Normal/Shear stiffness (N/mm ³)	–	–	–	140/60	–	70/30
		Tensile strength (N/mm ²)	–	–	–	0.21	–	0.21
	Tensile behaviour (exponential softening)	Mode-I fracture energy (N/mm)	–	–	–	0.01	–	0.01
		Cohesion (N/mm ²)	–	–	–	0.21	–	0.21
	Shear behaviour (exponential softening)	Friction angle (rad)	–	–	–	0.523	–	0.523
		Mode-II fracture energy (N/mm)	–	–	–	0.105	–	0.105
	Compressive behaviour (hardening-softening)	Compressive strength (N/mm ²)	–	–	–	16	–	16
		Compressive fracture energy (N/mm)	–	–	–	31.5	–	31.5

^a The values of the input parameters are from the experimental records [14,16] or are calibrated according to recommendations from the literature [48,49].

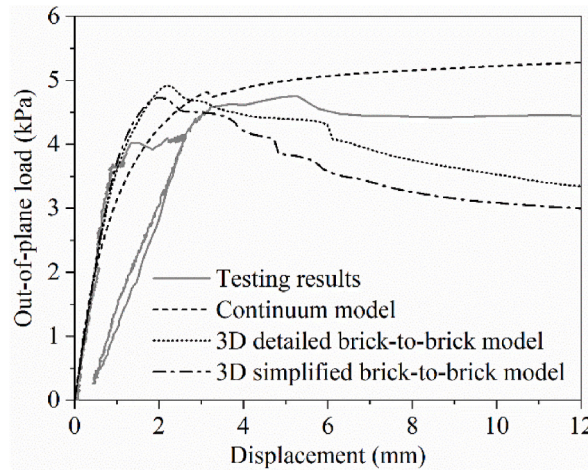


Fig. 11. Load-displacement curves of various modelling approaches.

$$\begin{Bmatrix} \sigma \\ \tau_s \\ \tau_t \end{Bmatrix} = \begin{bmatrix} k_{nn} & 0 & 0 \\ 0 & k_{ss} & 0 \\ 0 & 0 & k_{tt} \end{bmatrix} \begin{Bmatrix} u \\ v_s \\ v_t \end{Bmatrix} \quad (6)$$

with k_{nn} and k_{ss} (k_{tt}) the normal and shear stiffness of the interface elements, respectively.

The tensile stress beyond the tensile strength f_t is assumed to soften exponentially (Fig. 6c):

$$\sigma = f_t e^{-\frac{f_t}{G_f^I} u} \quad (7)$$

with G_f^I the Mode-I fracture energy.

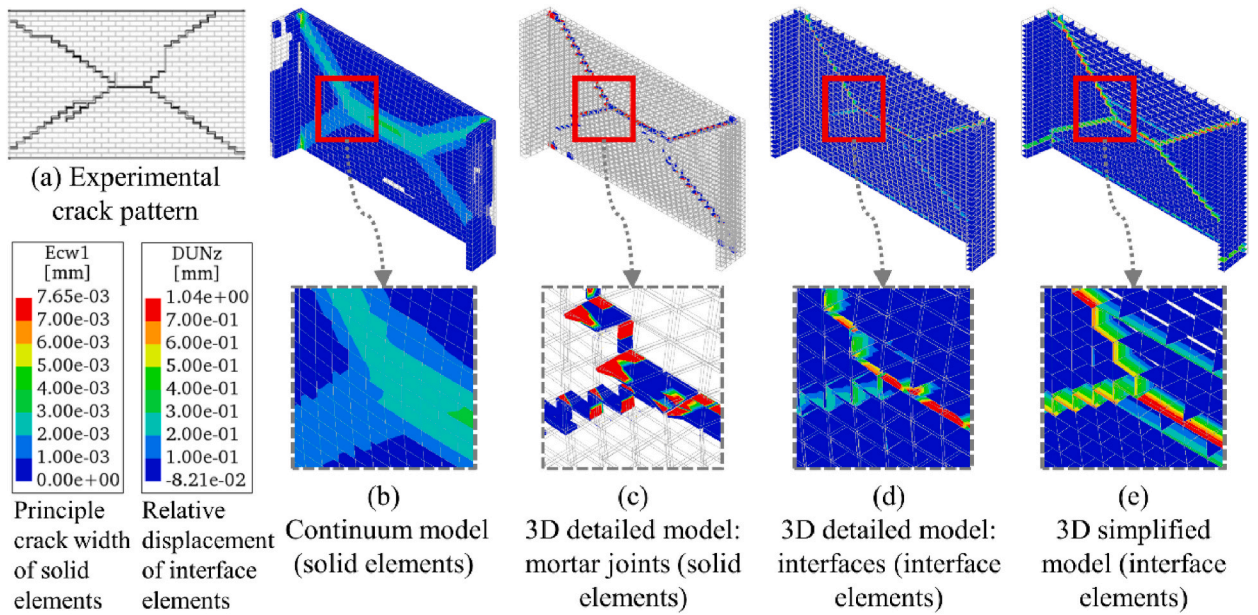


Fig. 12. Comparison of the crack patterns from various modelling approaches. Crack patterns are taken when the wall central point reaches a displacement of 8 mm. Deformation scale factor: 20.

Table 6
Comparison of the computational efficiency of the modelling approaches.

Modelling approach	Continuum model	3D detailed brick-to-brick model	3D simplified brick-to-brick model
Number of solid elements	4089	14,535	4089
Number of interface elements	-	25,662	5775
Time to reach a displacement of 8 mm ^a	1 h 9 min	23 h 15 min	4 h 18 min

^a The processor of the employed desktop is Intel(R) Xeon(R) CPU E5-1650.

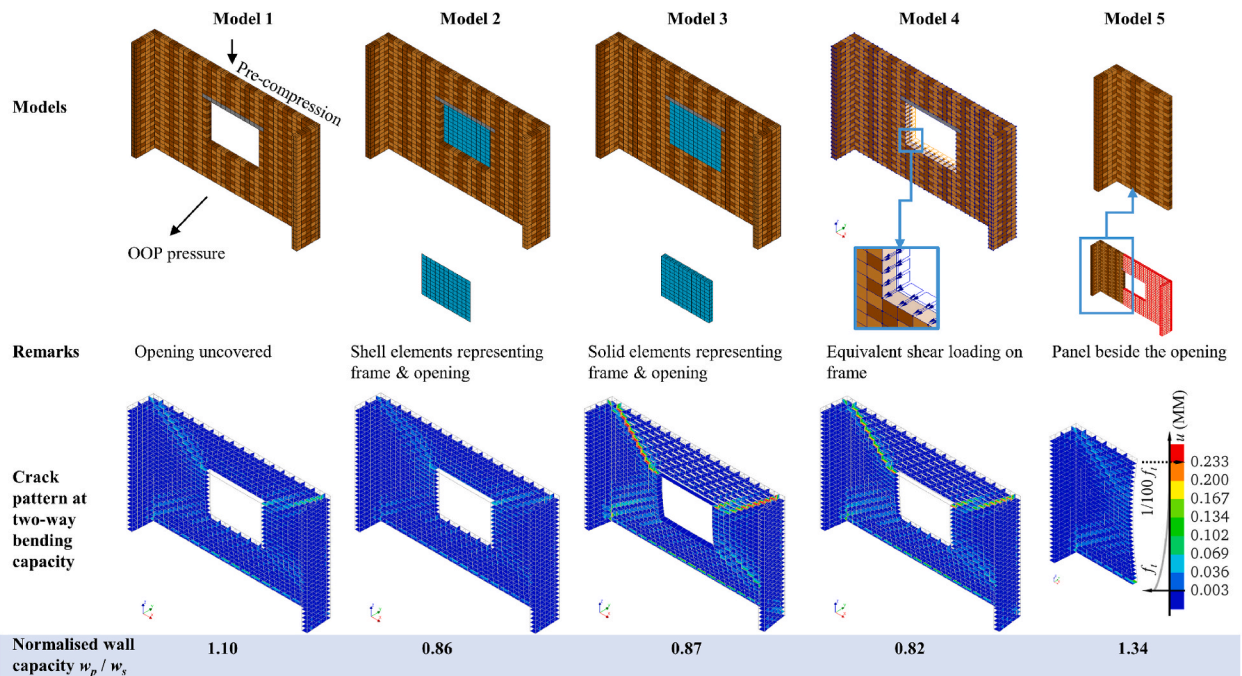


Fig. 13. Numerical models considering various arrangements of the opening area and corresponding modelling results. Deformation scale factor: 50.

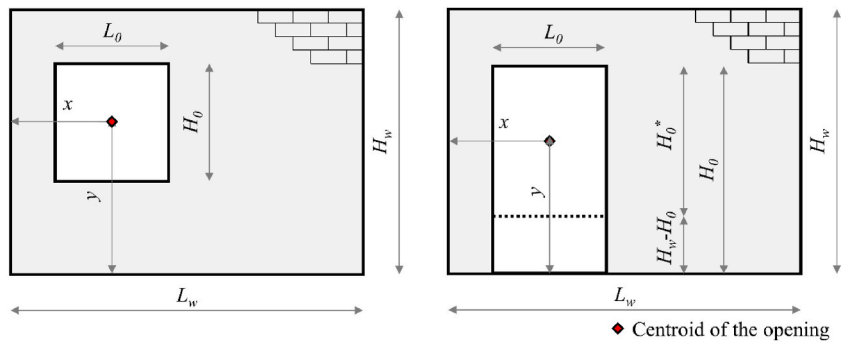


Fig. 14. Geometric parameters related to the wall with a window or door.

The Coulomb friction mode is described by:

$$\tau = \sigma \cdot \tan \varphi + c \tag{8}$$

where c is the cohesion of the brick-mortar interface and φ is the friction angle.

The initial cohesion of the interface softens exponentially (Fig. 6d):

$$c = c_0 e^{-\frac{v_0}{G_f^H} v} \tag{9}$$

with c_0 and G_f^H the initial cohesion of the brick-mortar interface and Mode-II fracture energy, respectively.

The compressive stress hardens till reaching the compressive strength f_c followed by softening. In this research, since very limited compressive failure was observed within mortar joints in the experiments, and also because the compressive strength of masonry is relatively high, the compressive failure in the numerical models is trivial.

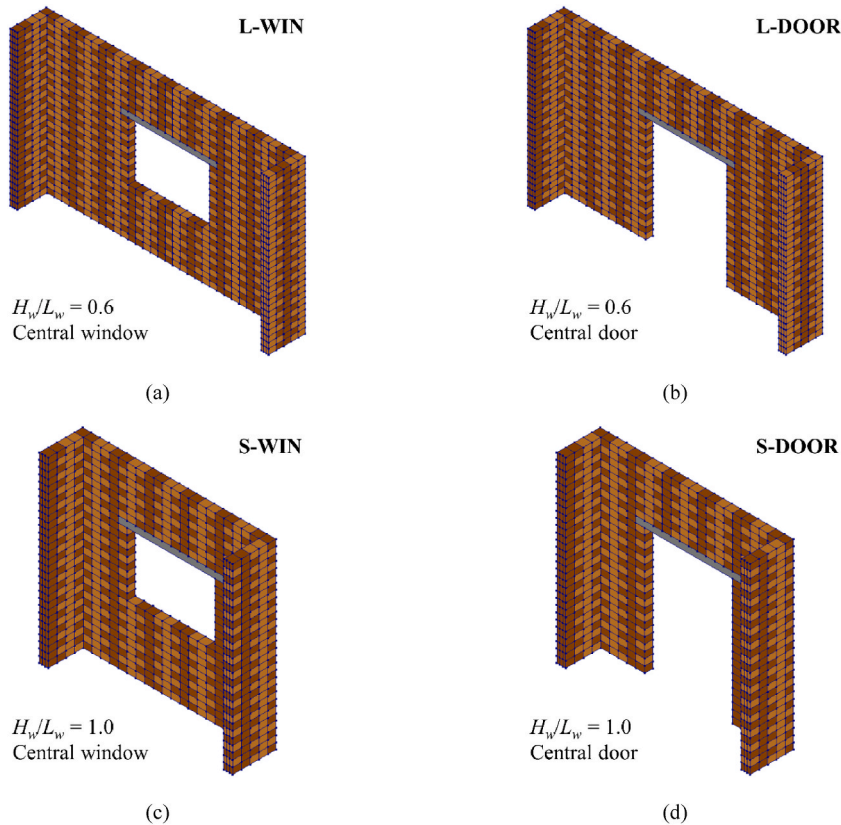


Fig. 15. Four types of models studying the influence of the opening size: (a) L-WIN, $H_w/L_w = 0.6$, central window; (b) L-DOOR, $H_w/L_w = 0.6$, central door; (c) S-WIN, $H_w/L_w = 1.0$, central window; (d) S-DOOR, $H_w/L_w = 1.0$, central door.

The rotating smeared cracking model (e.g. Refs. [42,43]) was used to simulate the cracking of the bricks. Due to the general absence of compression failure in bricks for OOP two-way bending experiments, a linear behaviour in compression was adopted for the bricks. In the tension regime, an exponential softening was adopted:

$$\sigma_1 = f_{bt} e^{-\frac{f_{bt}}{G_{f,b}^I} \varepsilon_1} \quad (10)$$

with σ_1 and ε_1 the stress and strain along the maximum principal direction, respectively; f_{bt} the tensile strength of bricks; $G_{f,b}^I$ the Mode-I fracture energy of the bricks, and h_{cr} the crack bandwidth.

Numerical modelling was carried out with the finite element software DIANA 10.4 [44]. Wall 1 was selected for calibration of the numerical model. Clay bricks were extended in dimensions from $230 \times 110 \times 76 \text{ mm}^3$ to $240 \times 110 \times 86 \text{ mm}^3$ and were modelled with 20-node quadratic solid elements. Mortar joints were modelled with zero-thickness 8-node quadratic interface elements. The mesh of the model was shown in Fig. 7a. A complete brick was meshed in 2, 1 and 3 divisions in length (l_w), height (h_w) and thickness (t_w) directions, respectively (Fig. 7b). At the intersections of the main wall and the return walls, half bricks were meshed in a refined manner ($3 \times 1 \times 3$ divisions) to avoid irregular meshed shapes (Fig. 7c). The mesh manner of the interface elements follows that of the brick surfaces (Fig. 7d).

Fig. 7a shows the boundary conditions of the model. The wall was restrained translationally in Y direction (OOP direction). The bottom face of the wall was connected to the environment using boundary interface elements that shared the same material properties as the other interface elements and were constrained along the Z direction. For the return walls, the translation along the Y direction was constrained at the central lines. Additionally, on the left return wall at the central lines, translations along X direction were constrained to prevent rigid body movements. Besides, the edges of the outer surfaces of the return walls were tied in X and Y directions so that these surfaces can keep plane when they rotate (Fig. 7a).

The wall was initially applied with self-weight and pre-compression in two sequential steps. Next, evenly distributed loads were applied to the exterior face of the main wall in fixed step sizes. This load was arc-length controlled with the Quasi-Newton iterative method. The central point of the main wall was selected as the control point.

The calibrated input parameters of the bricks and interface elements are summarised in Table 2 and Table 3, respectively. More details regarding the calibrating procedure can be found in Ref. [22].

4.3. Calibration and validation of the numerical models

The calibration and validation of the numerical models are based on the solid Wall 1 and the perforated Wall 3 from Ref. [14], respectively. The numerical models share identical settings. For Wall 3, the opening was left non-covered and non-loaded; only the masonry part was loaded. The results are shown in Fig. 8 in terms of the out-of-plane pressure versus out-of-plane displacement. The calibration shows that the numerical model matches well with the testing results in terms of initial stiffness, two-way bending capacity and crack pattern. This suggests that the boundary conditions and materials are accurately calibrated. The numerical model is validated by the simulations of Wall 3 (Fig. 8b and d). On the other hand, the post-peak pressure drops more sharply than that in the experiment. This phenomenon has also been observed by Karimi Ghaleh Jough and Golhashem [45] who also used the 3D simplified brick-to-brick modelling approach to predict the two-way bending capacity of URM walls in OOP two-way bending. In fact, according to the shake-table tests by Graziotti et al. [17] and monotonic static tests by Lawrence [46] on the URM walls in OOP two-way bending, the wall capacity decreased sharply after reaching the peak. The model validation is here reported for perforated walls, namely Wall 4–8 from the same testing campaign. Fig. 9 shows that the numerical models precisely capture the crack patterns of the walls.

Table 7

All cases corresponding to four modelling types.

Long walls with windows (L-WIN)			Long walls with doors (L-DOOR)		
Case	Opening area ^a (mm ²)	Opening size η ^b	Case	Opening area (mm ²)	Opening size η
L-WIN-SZ1	840 × 602	0.21	L-DOOR-SZ1	840 × 1548	0.21
L-WIN-SZ2	1080 × 774	0.27	L-DOOR-SZ2	1080 × 1634	0.27
L-WIN-SZ3	1320 × 946	0.33	L-DOOR-SZ3	1320 × 1720	0.33
L-WIN-SZ4	1560 × 1118	0.39	L-DOOR-SZ4	1560 × 1806	0.39
L-WIN-SZ5	1800 × 1290	0.45	L-DOOR-SZ5	1800 × 1892	0.45
L-WIN-SZ6	2040 × 1462	0.52	L-DOOR-SZ6	2040 × 1978	0.52
L-WIN-SZ7	2280 × 1634	0.58	L-DOOR-SZ7	2280 × 2064	0.58
L-WIN-SZ8	2520 × 1806	0.64	L-DOOR-SZ8	2520 × 2150	0.64
Short walls with windows (S-WIN)			Short walls with doors (S-DOOR)		
Case	Opening area (mm ²)	Opening size η	Case	Opening area (mm ²)	Opening size η
S-WIN-SZ1	720 × 516	0.30	S-DOOR-SZ1	720 × 1548	0.30
S-WIN-SZ2	960 × 688	0.40	S-DOOR-SZ2	960 × 1634	0.40
S-WIN-SZ3	1200 × 860	0.50	S-DOOR-SZ3	1200 × 1720	0.50
S-WIN-SZ4	1440 × 1032	0.60	S-DOOR-SZ4	1440 × 1806	0.60
S-WIN-SZ5	1680 × 1204	0.70	S-DOOR-SZ5	1680 × 1892	0.70
S-WIN-SZ6	1920 × 1376	0.80	S-DOOR-SZ6	1920 × 1978	0.80

^a Opening area: $H_0 \times L_0$

^b Opening size: $\eta = L_0/L_w$

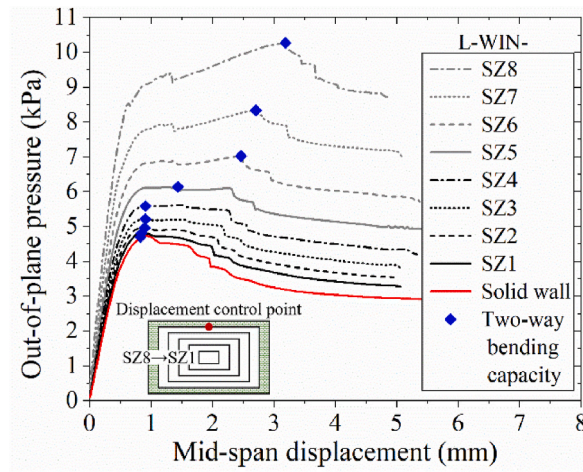


Fig. 16. Out-of-plane pressure versus mid-span displacement of L-WIN cases. For all cases, the mid-span displacement is calculated at the location of the control point for wall L-WIN-SZ8 (red dot in the figure above). (For interpretation of the references to colour in this figure legend, the reader is referred to the Web version of this article.)

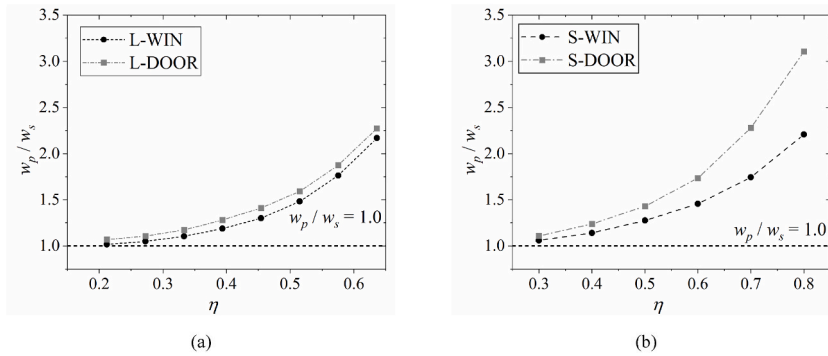


Fig. 17. The influence of the opening size η on the normalised two-way bending capacity: (a) for long walls (L-WIN and L-DOOR); (b) for short walls (S-WIN and S-DOOR).

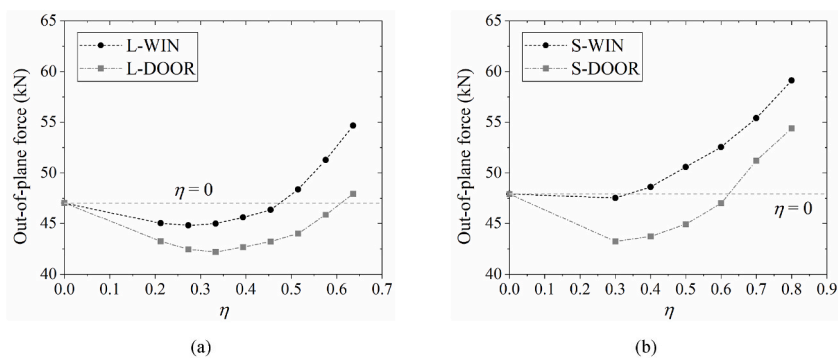


Fig. 18. The influence of the opening size η on the out-of-plane force: (a) of long walls (L-WIN and L-DOOR); (b) of short walls (S-WIN and S-DOOR).

Additionally, the numerical models predict the two-way bending capacity to a quite reasonable extent, with a Mean Absolute Percentage Error of 11% (see Table 4). Therefore, the numerical model is considered to be suitable for this study. For more details about the calibration and validation of the numerical models, readers are referred to Ref. [22].

4.4. Comparison with other modelling approaches

In this section, the results of the 3D simplified brick-to-brick modelling are compared with those of the other two commonly used

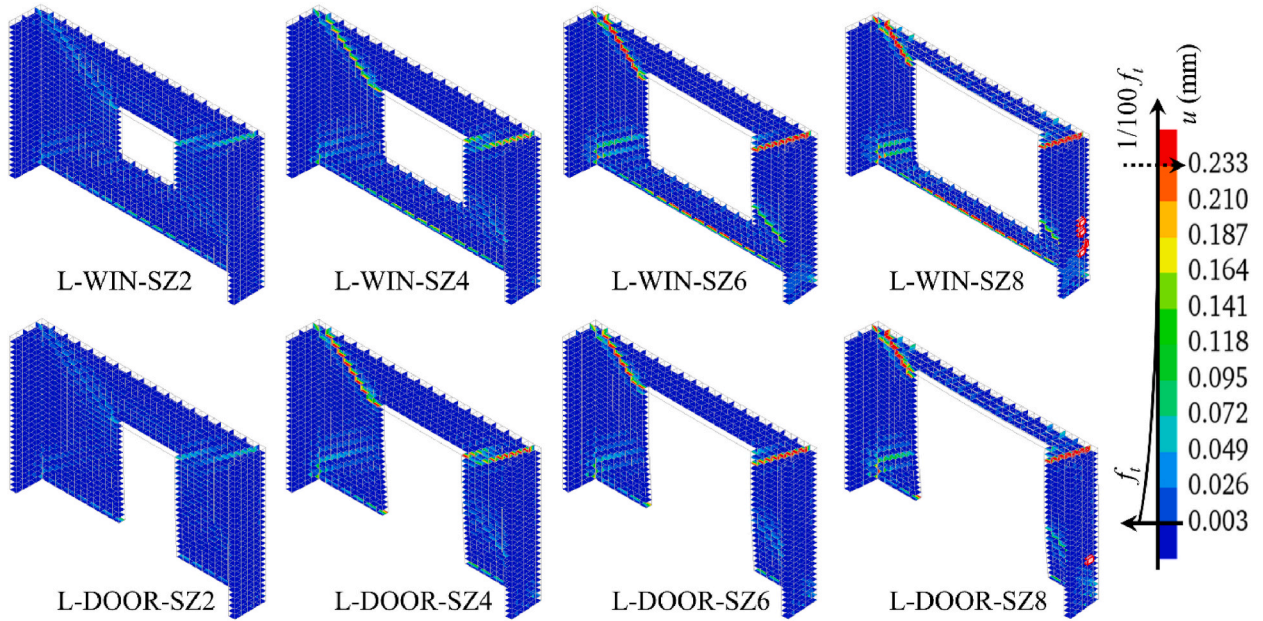


Fig. 19. Cracking patterns of selected cases of modelling types L-WIN and L-DOOR at the two-way bending capacity.

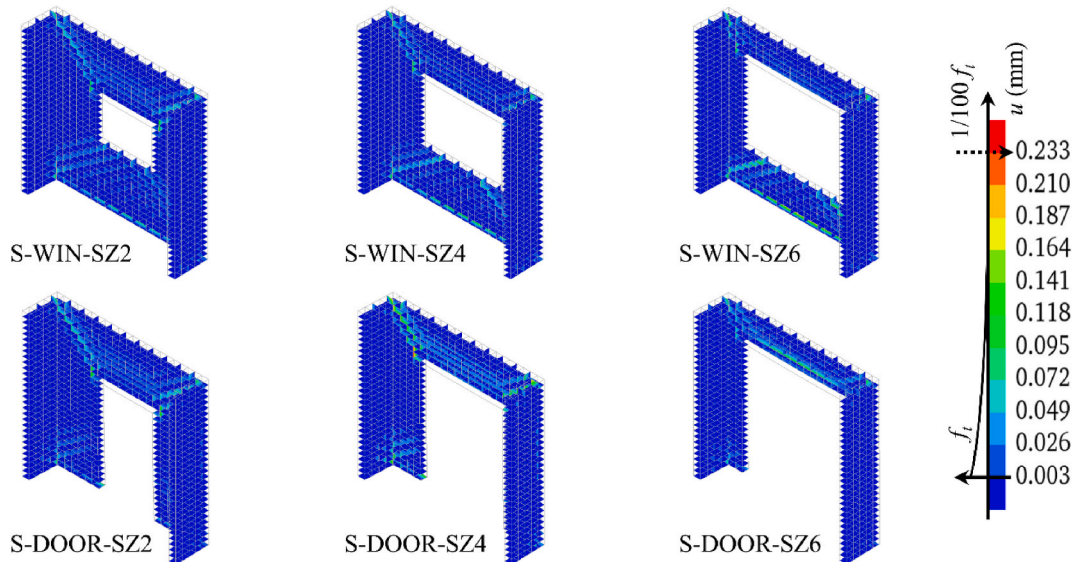


Fig. 20. Crack patterns of selected cases of modelling types S-WIN and S-DOOR at the two-way bending capacity.

modelling approaches, namely, continuum modelling and 3D detailed brick-to-brick modelling. With the continuum modelling, bricks and mortar joints are not distinguished, and the masonry structure is modelled as a continuum body. With the detailed brick-to-brick modelling, both mortar joints, bricks and interfaces between them are modelled according to real dimensions [47]. The comparison is based on the solid Wall 1 used for the model calibration in Section 4.3. The mesh size, geometry, boundary and loading conditions are kept unchanged. The geometry of models and zoom-in view of masonry constituents are presented in Fig. 10. Regarding the constitutive models, for the 3D detailed brick-to-brick modelling, the combined cracking-shearing-crushing model is assigned to the interfaces between mortar joints and bricks, while the rotating smeared cracking model is assigned to the mortar joints and bricks. For the masonry in the continuum model, the rotating smeared cracking model is assigned. The input parameters for the constitutive models are from the experimental records [14,16] or are calibrated according to recommendations from the literature [48,49]. Details about the input parameters are listed in Table 5. Note this section aims to simply compare the computational efficiency and the ability to capture the crack patterns of the modelling approaches. A comprehensive comparison is out of the scope of this study and is suggested to be investigated in separate research.

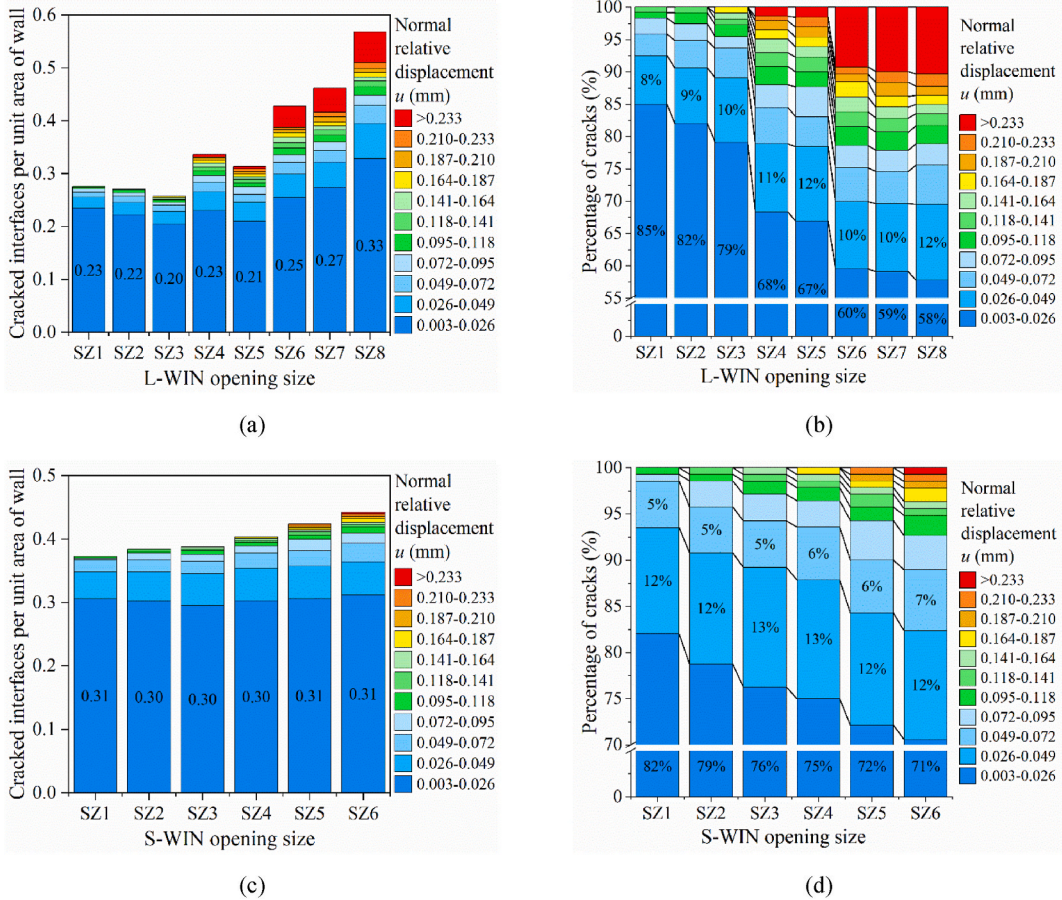


Fig. 21. The area of the cracked interfaces per unit wall area of (a) L-WIN and (c) S-WIN cases; the percentage of each grouped cracked interfaces per unit wall area of (b) L-WIN and (d) S-WIN cases.

Fig. 11 presents the load-displacement curves of various modelling approaches. The continuum model predicts a lasting increase of load after the peak, which is against the testing results. The 3D detailed and simplified brick-to-brick models predict similar trends about the load-displacement relations and are closer to the testing results. Note that varying the input parameters of the constitutive models can result in different load-displacement curves, but will not change the general crack patterns predicted by the modelling approaches. Fig. 12b shows that with the continuum model, the crack patterns are roughly presented in several wide banded areas on the wall surface. By contrast, both the simplified and detailed brick-to-brick modelling can locate the cracks between the bricks therefore precisely predicting the crack patterns (Fig. 12c–e). The detailed modelling can further predict the failure of mortar joints that are not modelled in the simplified modelling (Fig. 12c). Table 6 compares the computational efficiency of the modelling approaches. When the central point of the wall reaches a displacement of 8 mm, the continuum model consumes the least time (1 h 9 min), the 3D simplified brick-to-brick model requires a longer period, over 4 h, while the 3D detailed modelling is almost 6 times slower than the simplified model (over 23 h). This can be explained by the number of elements in various models. Though the meshing size is the same among the models, the continuum model consists of the least number of elements, since only solid elements are necessary. By contrast, the simplified model has not only an equivalent number of solid elements as the continuum model but also an extra amount of interface elements, which significantly increases the computing time. The numbers of the solid and interface elements of the detailed model are nearly 4 and 5 times those of the simplified model, respectively. This is because the mortar joints and adhesions between the bricks and mortar joints are both modelled in the detailed model, which significantly increases the amount of the elements. Besides, all the elements are assigned with physical nonlinearity. Therefore, the detailed model consumes much longer time than the other two approaches. Overall, the 3D simplified brick-to-brick modelling is the most suitable for the scope of this research, considering its ability to precisely capture the crack patterns in URM walls with a reasonable computational time.

5. Various arrangements of the opening area

To examine the effect of different arrangements of the opening area on the two-way bending capacity of URM walls, five numerical models labelled Model 1–Model 5 were created, as shown in Fig. 13. The modelling configurations were the same as those in Section 4. In Model 1 the opening was non-covered and non-loaded, which follows Wall 3 in Griffith and Vaculik’s experiments [14]. In Model 2,

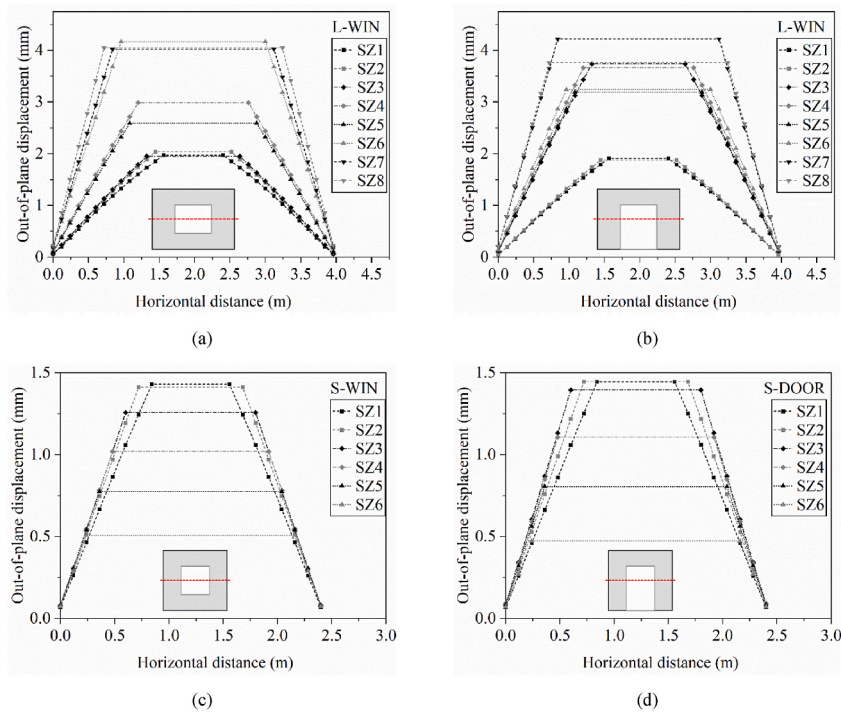


Fig. 22. Deformation profiles at the mid-height of walls reaching the two-way bending capacity: (a) L-WIN; (b) L-DOOR; (c) S-WIN; (d) S-DOOR.

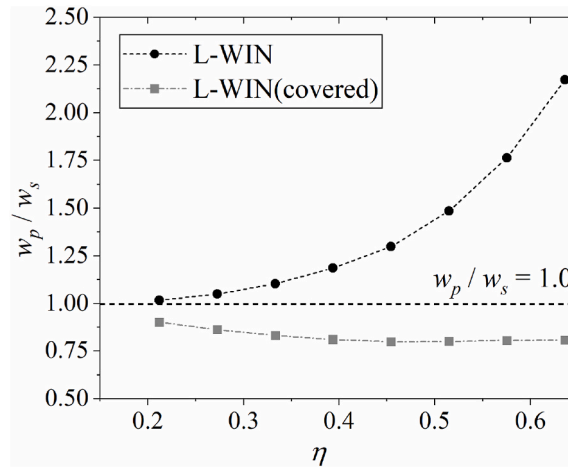


Fig. 23. Comparisons between different scenarios.

the outer face of the opening area was covered with linear elastic shell elements of which the thickness was set as 18 mm and the elastic modulus was set as 10,000 N/mm². These mechanical attributes follow those of a timber plate, as in Ref. [11]. In Model 3, shell elements were replaced with solid elements of which the elastic modulus was set as 1000 N/mm². The opening was connected with the wall via interface elements. This arrangement takes the interaction between the opening frame and the masonry part into account. In Model 4, an equivalent load, q_{eq} was applied to four faces along the surrounding area of the opening. This arrangement is similar to that from the YLM calculation by Baker et al. [32]. The equivalent load q_{eq} was calculated by

$$q_{eq} = \frac{q \cdot H_0 \cdot L_0}{2(H_0 + L_0)t_w} \tag{11}$$

where q is the load applied to the wall; H_0 and L_0 are the opening height and length, respectively; t_w is the wall thickness. Model 5 simulates the behaviour of the panel beside the opening as an independent C shape wall (one vertical edge free); this aims at examining additional checks required by the Australian Standard (article 7.4.4.1 (e) in Ref. [25]).

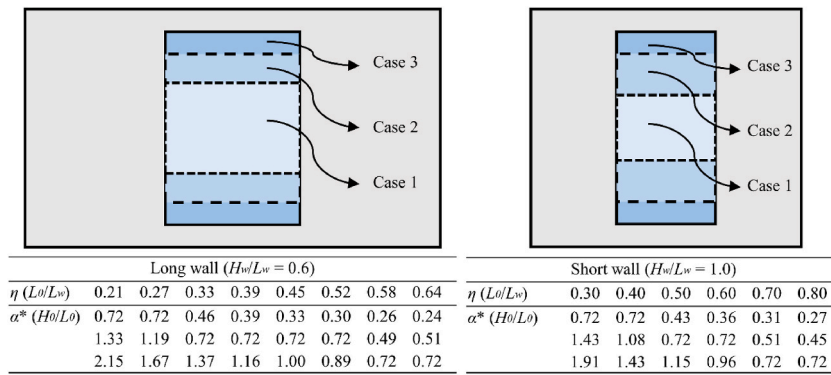


Fig. 24. Sketches of models and cases with respect to the influence of opening shape.

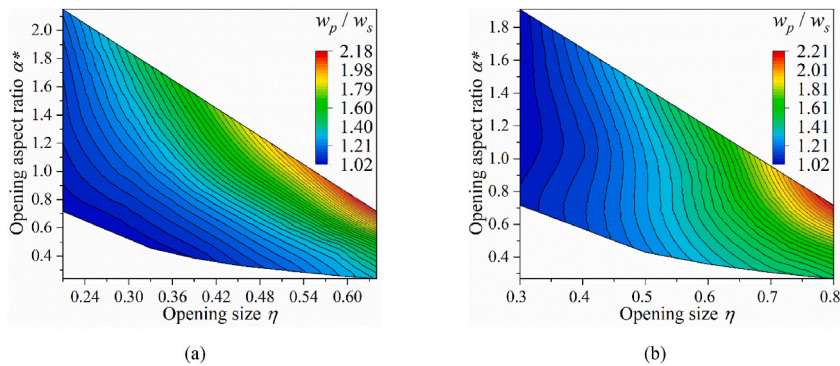


Fig. 25. Influence of the opening shape on the two-way bending capacity. Cases based on (a) L-WIN; (b) S-WIN. The contour plots are interpolated based on the data boundary.

The modelling results are presented in Fig. 13. The normalised two-way bending capacity of the perforated wall to the solid wall (w_p/w_s) shows that if the opening area is non-covered, the presence of the opening increases the two-way bending capacity, as observed from Model 1. If the panel beside the opening is independently considered, as in Model 5, the two-way bending capacity is even higher than that of Model 1. In contrast, the two-way bending capacity reduces if the opening area is covered and loaded, even though the opening is covered in different ways, as shown in Model 2, 3 and 4. The crack pattern shows that if the opening is non-covered, the diagonal cracks do not develop sufficiently at two-way bending capacity, as shown in Model 1 and 5. Differently, in Model 3 and 4, the diagonal cracks develop more sufficiently at two-way bending capacity. While in Model 2, diagonal cracks develop slightly at two-way bending capacity, even though its opening area is covered as in Model 3. The differences among the crack patterns are attributed to different local failure mechanisms triggered by the arrangement of the opening area. Overall, the numerical models validate the contradictory trends of the influence of openings on the two-way bending capacity caused by various arrangements of the opening area, as observed from experimental results and YLM evaluations.

6. Influence of opening

In this section, the influence of the opening on the two-way bending capacity of URM walls is numerically studied. The opening areas are non-covered and non-loaded in numerical models as in Model 1 in Section 5. This arrangement is considered because in seismic scenarios, dynamic loads majorly take effect on the masonry part rather than the opening since the mass of the former is much larger than the latter. Three parameters related to the opening, i.e. size, shape and position, which can fully determine the opening geometry, are explored separately. As shown in Fig. 14, these parameters are defined in the following ways in this study. The opening size is defined as the normalised length of the opening to that of the wall ($\eta = L_0/L_w$). The opening shape is defined as the aspect ratio ($\alpha^* = H_0/L_0$) for windows. For doors, a nominal height H_0^* is defined as $(2H_0 - H_w)$, which is equivalent to the height of a window located at the mid-height of the wall. In this way, the aspect ratio of the doors is defined as ($\alpha^* = H_0^*/L_0$) which makes the shape and position of the doors comparable to those of the windows. The opening position is defined as the normalised horizontal and vertical distances from the opening centroid to the left and bottom edges of the wall, respectively:

$$\lambda_x = \frac{x - L_0/2}{L_w - L_0} \quad x \in \left(\frac{L_0}{2}, L_w - \frac{L_0}{2} \right) \tag{12}$$

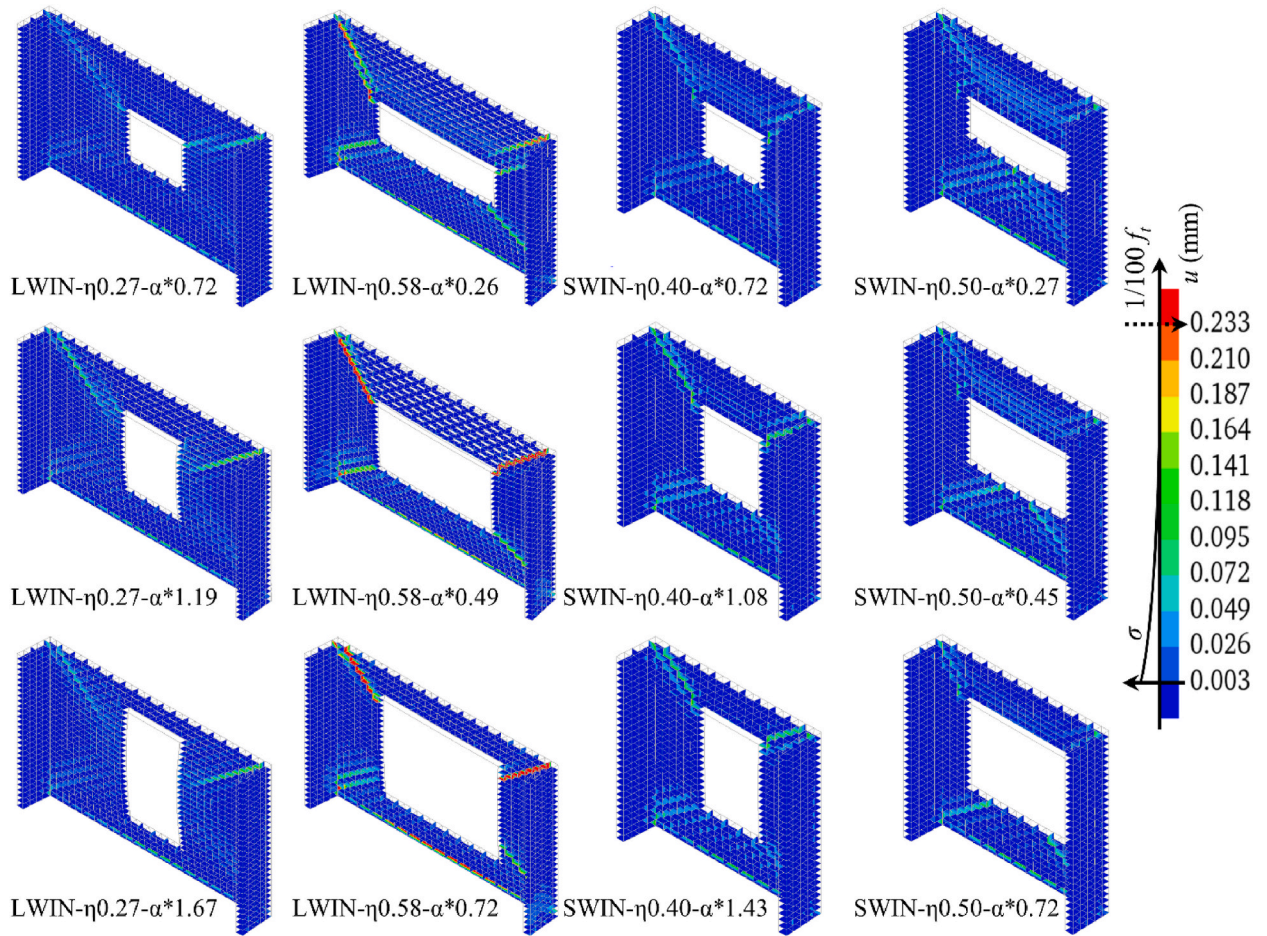


Fig. 26. Influence of the opening shape on the crack pattern.

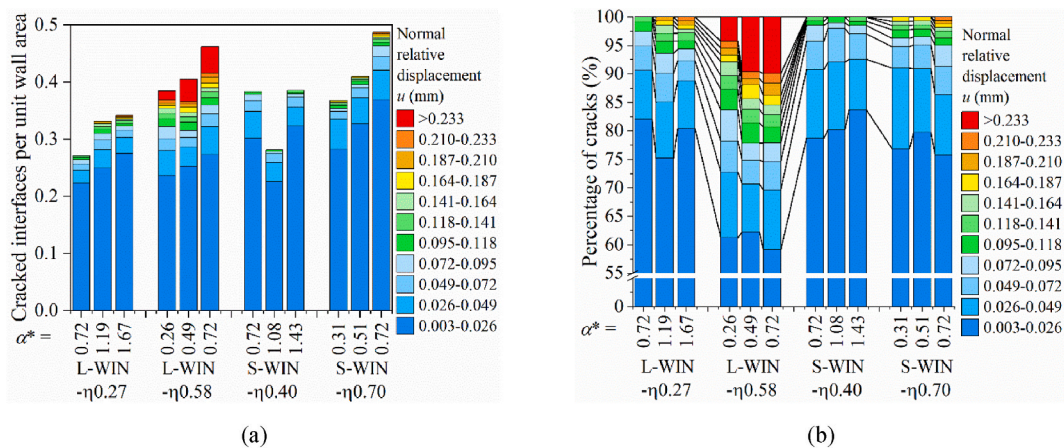


Fig. 27. Area of the cracked interfaces (a) and the percentage of each grouped cracked interfaces (b) per unit wall net area of selected cases.

$$\lambda_y = \frac{y - H_0/2}{H_w - H_0} \quad y \in \left(\frac{H_0}{2}, H_w - \frac{H_0}{2} \right) \tag{13}$$

where x and y are the absolute horizontal and vertical distances from the opening centroid to the left and bottom edges of the wall, respectively. With this definition, both λ_x and λ_y range from 0 to 1.

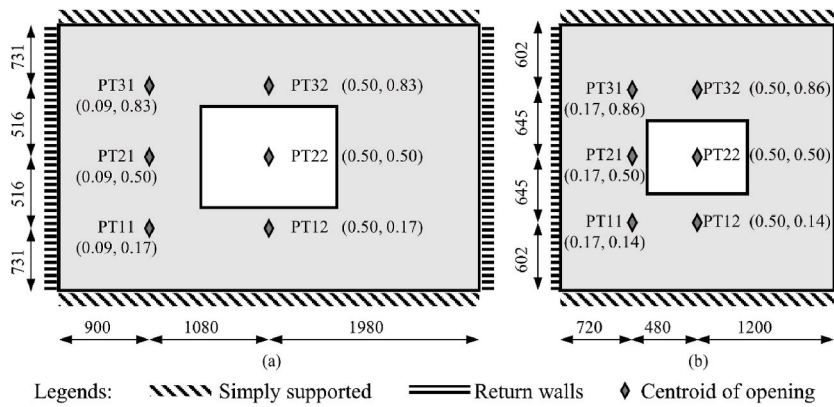


Fig. 28. Modelling cases exploring the influence of opening position based on (a) L-WIN-SZ3; (b) S-WIN-SZ2.

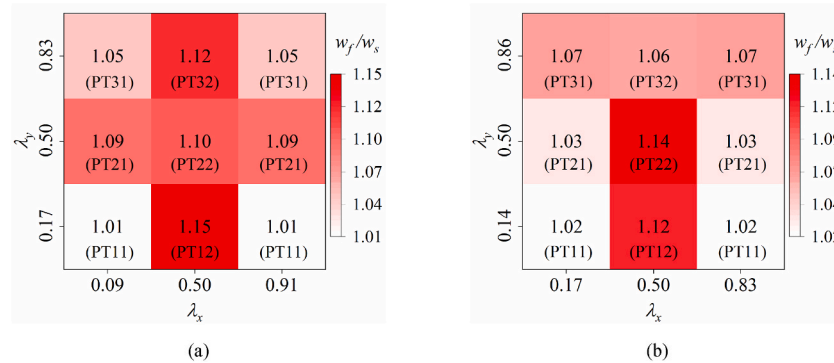


Fig. 29. Influence of opening position on two-way bending capacity. Cases based on (a) L-WIN-SZ3; (b) S-WIN-SZ2.

6.1. Influence of opening size

6.1.1. Modelling types and cases

Four modelling configurations were designed to study the influence of the opening size, as shown in Fig. 15. The modelling configurations are labelled in such ways: L and S denote a long wall with an aspect ratio (H_w/L_w) of 0.6 and a short wall with an aspect ratio of 1.0, respectively; WIN and DOOR denote a central window and central door, respectively. For each configuration, different opening sizes were considered, as shown in Table 7. The aspect ratios of the windows and doors are constant according to previous definitions.

6.1.2. Influence of opening size on the two-way bending capacity

The OOP pressure versus the mid-span displacement curves of L-WIN cases are shown in Fig. 16. In this figure, the OOP pressure is shown with regard to the wall net area. The middle point of the top edge of L-WIN-SZ8 is selected as the displacement control point. The control points of the other cases are of the same position on the walls. Fig. 16 shows that as the opening size increases, both the initial stiffness and the two-way bending capacity of the wall increase. Besides, at the same position of all walls (red dot, namely the displacement control point marked in Fig. 16), when reaching the two-way bending capacity, the deflection becomes larger as the opening size increases. This finding is counter-intuitive but is in accordance with similar numerical studies by Nasiri and Liu [23] and Liberatore et al. [50]. The influence of the opening size (η) on the two-way bending capacity is shown in Fig. 17. The two-way bending capacity in terms of pressure on the net area of the perforated wall is normalised by dividing the capacity of the corresponding solid wall. The figure shows that, assuming that the opening area is non-covered and non-loaded, increasing the opening size leads to an increase of the two-way bending capacity at an approximately exponential pace regardless of the wall aspect ratio and the opening type (window or door). For all cases the trend is similar. For long walls ($H_w/L_w = 0.6$), given a certain opening size, the normalised two-way bending capacity increases slightly when windows are replaced by doors, as shown in Fig. 17a. In contrast, for the short walls ($H_w/L_w = 1.0$), as the opening size increases, the two-way bending capacity of the wall with a door increases a bit more as compared to that of the wall with a window (Fig. 17b). In Fig. 18, the influence of the opening size on the OOP force is compared. The OOP force is calculated as two-way bending capacity timing the wall net area. Fig. 18 shows that for all four modelling types, compared with the solid wall, the OOP force decreases firstly as the opening size increases. When the opening size increases to a certain degree, the OOP force increases as the opening size increases, even though the wall net area keeps reducing.

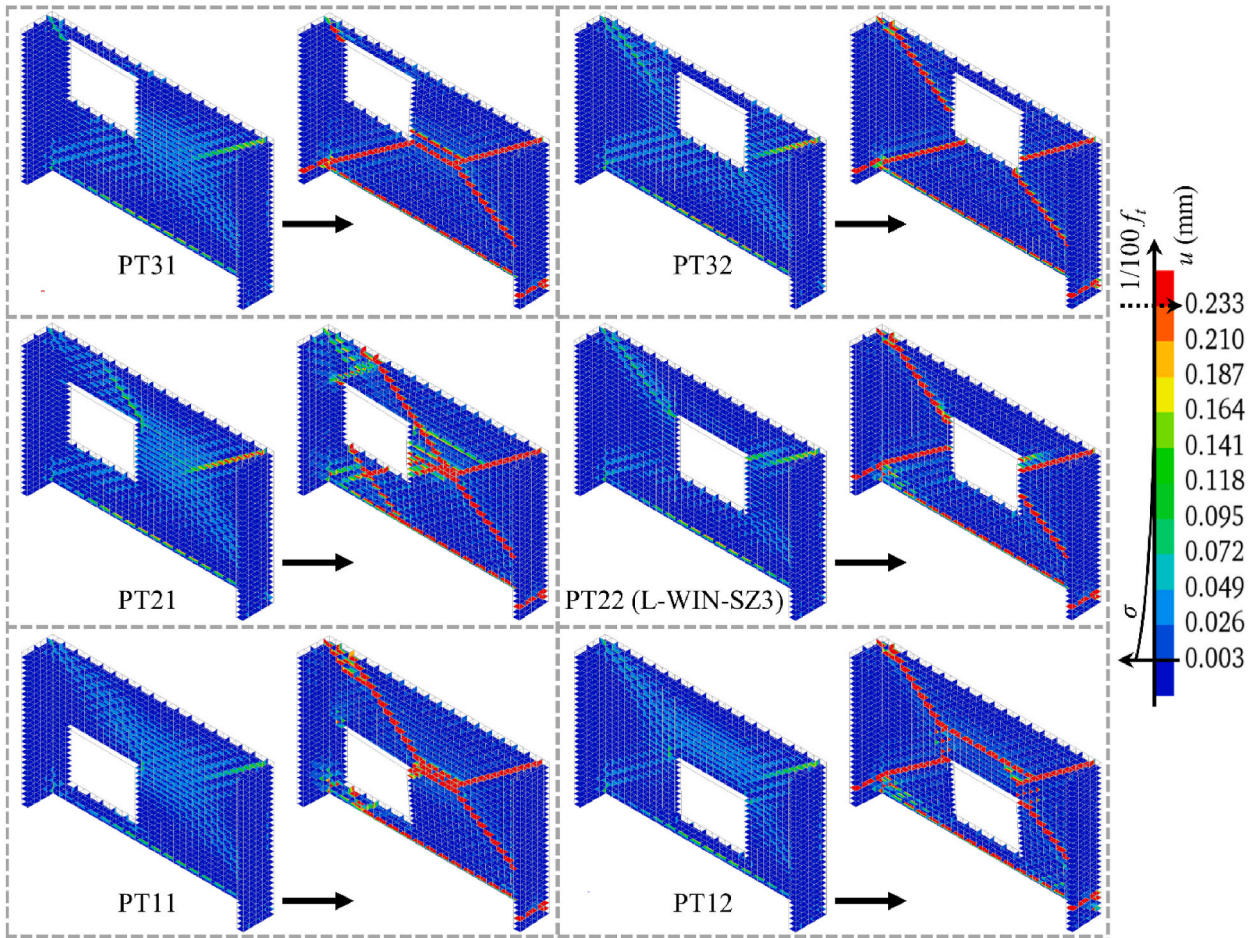


Fig. 30. The influence of the opening position on the crack pattern of the long walls (L-WIN-SZ3). Within each grey-dot-lined box, the crack patterns at the two-way bending capacity and the end of the analysis are shown to the left and right, respectively.

6.1.3. Influence of opening size on crack pattern

Fig. 19 and Fig. 20 present the crack patterns of selected cases at the two-way bending capacity. In these figures, cracks start to develop when the normal relative displacement (crack width u) is larger than 0.003 mm; cracks are considered to be fully developed when the tensile stress reduces to 1% of the tensile strength, which corresponds to a crack width u of 0.233 mm. For all cases of each modelling configuration, the presence of an opening does not alter the positions of the major diagonal cracks and horizontal bottom cracks. Different trends are observed between the long and short walls. For the long walls, as the opening size increases, the diagonal cracks on the top corners have more fully opened, and multiple diagonal cracks appear around the bottom corners. In contrast, these trends are relatively subtle concerning the short walls.

The area of the cracked interfaces per unit wall area of L-WIN and S-WIN cases are shown in Fig. 21 a and c, respectively. For each wall, the cracked interfaces were grouped by the normal relative displacement (u) considering partially cracked ($0.003 \text{ mm} < u < 0.233 \text{ mm}$) and fully cracked ($u > 0.233 \text{ mm}$) interfaces. The gross area of each cracked interfaces group was divided by the wall net area. Results show that for both the long and short walls, the summed area of the cracked interfaces per unit wall area increases as the opening size increases. The increment for the long walls is larger than that for the short walls. For all cracked interfaces with regard to each wall, the percentages of each grouped cracked interfaces per unit wall area are shown in Fig. 21 b and d for L-WIN and S-WIN cases, respectively. Results show that as the opening size increases, within per unit wall area, the percentage of the cracked interface with large normal relative displacement ($u > 0.210 \text{ mm}$) increases, while the percentage of the cracked interface with smaller normal relative displacement decreases ($0.003 \text{ mm} < u < 0.026 \text{ mm}$) or remained constant ($0.026 \text{ mm} < u < 0.072 \text{ mm}$). The results presented in Fig. 21 imply that as the opening size increases, more cracks have fully opened per unit area of the wall, therefore dissipating more fracture energy and leading to a higher two-way bending capacity.

6.1.4. Influence of opening size on deformation profile

At the two-way bending capacity, deformation profiles at the mid-height of the walls with openings non-covered are presented in Fig. 22. For long walls ($H_w/L_w = 0.6$), deformation at mid-height generally increases as the opening size increases (Fig. 22a), although some deviations are shown for walls with similar opening size, e.g. SZ1-SZ3 of L-WIN and SZ3-SZ6 of L-DOOR. In contrast with the long

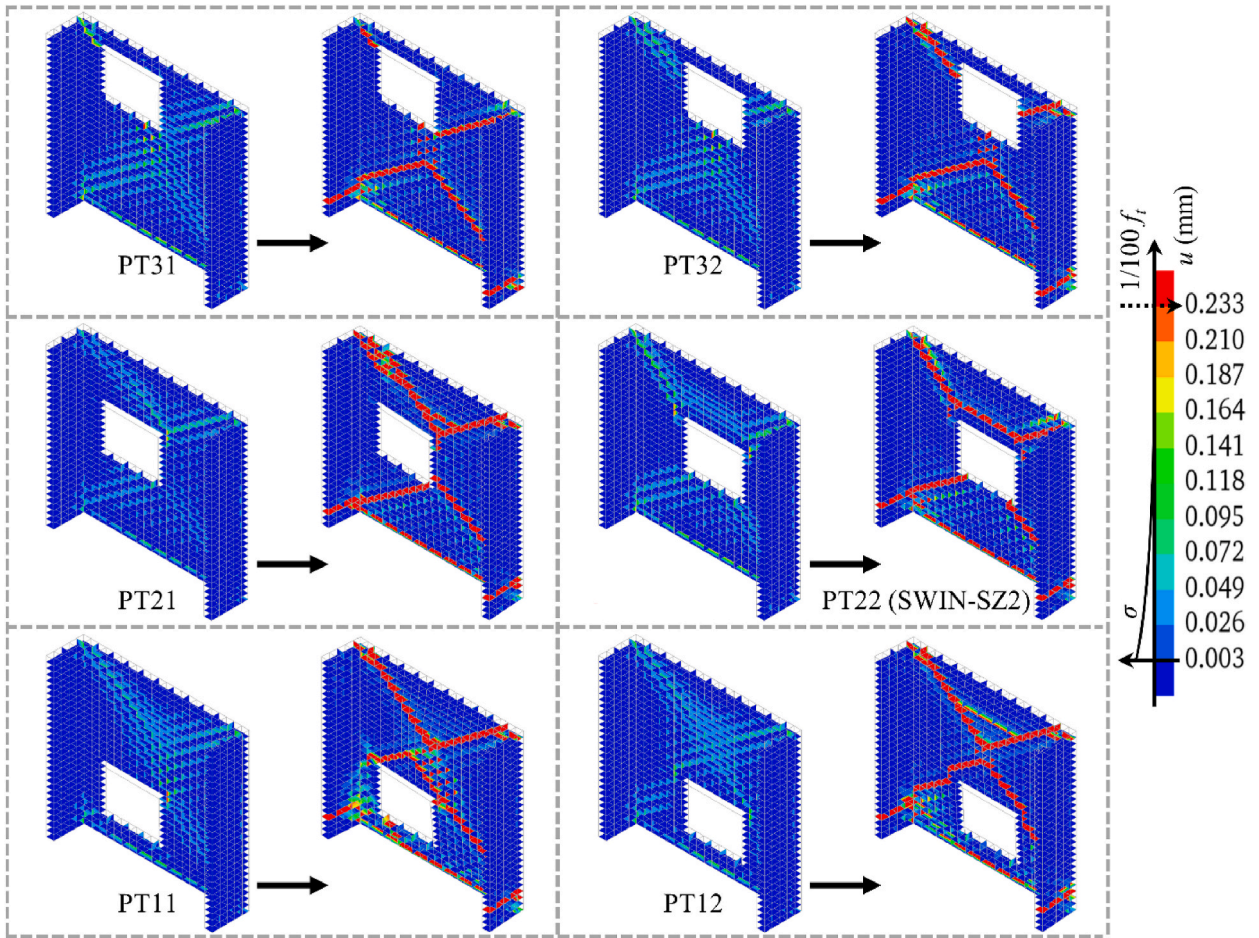


Fig. 31. The influence of the opening position on the crack pattern of the short walls (S-WIN-SZ2). Within each grey-dot-lined box, the crack patterns at the two-way bending capacity and the end of the analysis are shown to the left and right, respectively.

walls, at the same position of the short walls ($H_w/L_w = 1.0$), the increase of the opening size only increases the deformation slightly. The deformation profile can be roughly related to the summed cracked interfaces per unit wall area. As the opening size increases, for the long walls, both the summed area of cracked interfaces per unit wall area and the deformation profile increase; for the short walls, these two variables only increase slightly.

6.1.5. Comparison of the influence of the opening size with different arrangements

In this section, the influence of opening size is studied considering the arrangement of covered and loaded opening areas. The cases of long walls with a window opening are considered (L-WIN). The loading of the opening area is simulated by equivalent loads along the surrounding surfaces of the opening (Model 4 in Section 5). Fig. 23 shows that when the opening area is loaded, as the opening size increases, the normalised two-way bending capacity w_p/w_s decreases followed by a constant value. The difference between these and previous results can be explained as follows. When the opening area is non-covered and non-loaded, as the opening size increases, the bending moments caused by the OOP loads distribute more evenly on the masonry part of the wall. Therefore, the initial stiffness and ductility of the wall increase. Consequently, the wall dissipates more energy, thus reaching a higher two-way bending capacity compared to the solid wall. In contrast, when the opening area is covered and loaded, extra high bending moments carried by the opening area are imposed on the wall. These bending moments are distributed by the masonry parts, which leads to the reduction of the normalised two-way bending capacity.

6.2. Influence of opening shape

6.2.1. Modelling types and cases

In this section, the influence of the opening shape is studied. Based on each case of the long and short wall with a central window (L-WIN and S-WIN) from Section 6.1.1, the aspect ratio of opening (α^*) was varied while the opening size (η) and position (λ_x, λ_y) were kept constant. In total, 42 cases were studied including 14 cases from Section 6.1.1. The sketches of models and aspect ratios of all cases are present in Fig. 24.

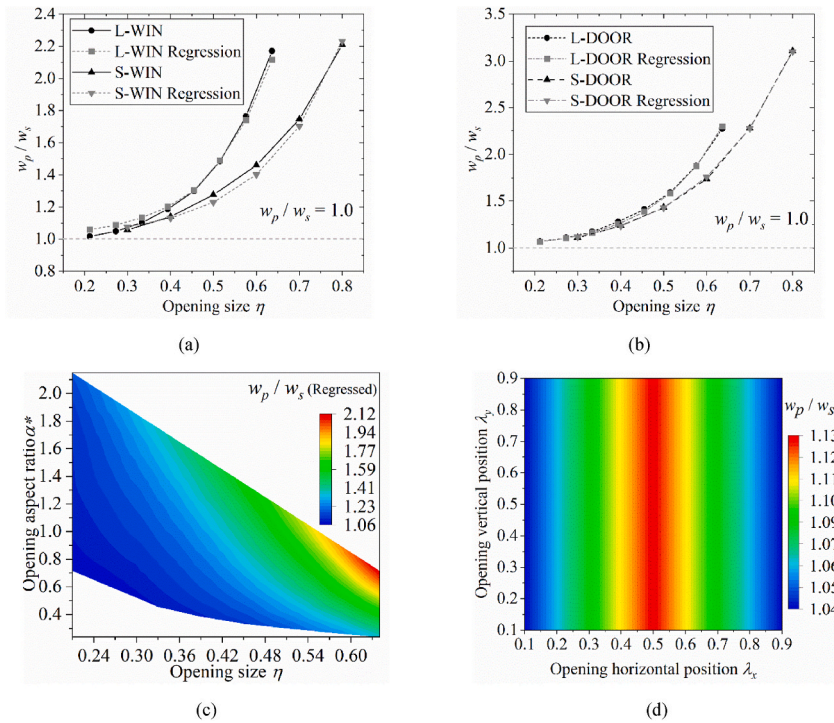


Fig. 32. Results of the proposed equations with regard to, (a) and (b): the wall aspect ratio/opening size considering a central window and door, respectively; (c) the aspect ratio and size of the opening; (d) the opening position.

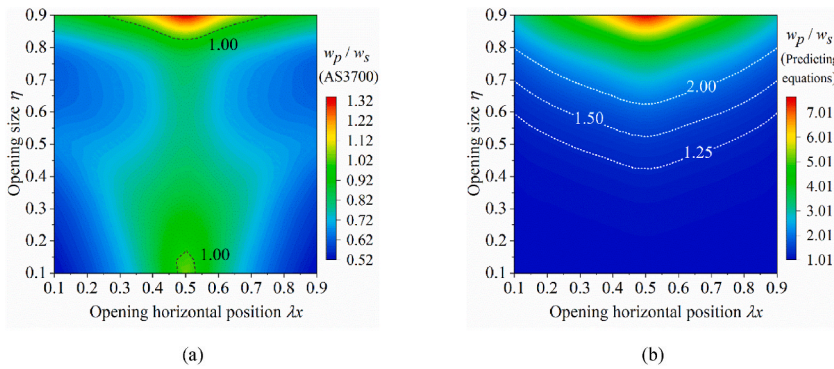


Fig. 33. Evaluations of the influence of the opening size and horizontal position on the two-way bending capacity by (a) AS3700 and (b) proposed equations.

6.2.2. Influence of opening shape on two-way bending capacity

The influence of the opening shape on the two-way bending capacity is shown in Fig. 25. For long walls, when the opening size is constant, the two-way bending capacity increases as the opening aspect ratio increases. Besides, this increasing effect is small when the opening size is small ($\eta = 0.27$), increasing the normalised two-way bending capacity (w_p/w_s) from 1.01 to 1.19 as the opening aspect ratio α^* increases from 0.72 to 2.15. In contrast, this increasing effect is relatively large when the opening size is large, increasing the normalised two-way bending capacity from 1.34 to 2.17 as the opening aspect ratio increases from 0.24 to 0.72. For short walls, when the opening size is smaller than 0.4, the two-way bending capacity decreases first then increases again as the opening aspect ratio increases. When the opening size is larger than 0.4, the two-way bending capacity constantly increases with the increase of the opening aspect ratio.

6.2.3. Influence of opening shape on crack pattern

The influence of the opening shape on the wall crack pattern at the two-way bending capacity is shown in Fig. 26. Cases of the long walls with the opening size of 0.27 and 0.58, and of the short walls with the opening size of 0.4 and 0.7 are selected. Each column presents cases with the same wall aspect ratio and opening size, but varied opening shape. A general tendency observed is that the locations of the major diagonal cracks remain the same as the opening shape changes. In some cases, secondary diagonal cracks, which

are parallel with the major diagonal cracks, can originate from the top corners of the openings, especially with short walls.

The area of the cracked interfaces and the percentage of each grouped cracked interfaces per unit wall area is presented in Fig. 27a and b, respectively. For long walls and short walls with large opening sizes, both the area of the cracked interfaces per unit wall net area and the percentage of larger cracked interfaces increases with the increase of the opening aspect ratio. In contrast, for short walls with a small opening, the area of the cracked interfaces per unit wall net area decreases first and then increases as the opening aspect ratio increases. This implies that by increasing the opening aspect ratio, a larger number of integration points are fully cracked; this results in a higher dissipation of fracture energy and results in a higher two-way bending capacity.

6.3. Influence of opening position

6.3.1. Modelling types and cases

The influence of the opening position is studied in this section. Two models, Type L-WIN-SZ3 and Type S-WIN-SZ2 from Section 6.1.1 were selected as reference models. For each reference model, the size and shape of the opening were constant, while the opening position varied. Since the walls are symmetric, the position of the opening only varies on one side. In Fig. 28, the cases are labelled as "PTXX", and the coordinates of the opening centroids are marked with (λ_x, λ_y) as defined at the beginning of Section 6.

6.3.2. Influence of opening position on two-way bending capacity

The influence of the opening position on the two-way bending capacity is presented in Fig. 29. Results of cases PT11, 21, and 31 are mirrored to the other symmetric half of the walls. Results show that the influence of the opening position on the two-way bending capacity is limited. For the long walls, the varying opening position causes the normalised two-way bending capacity to change between 1.01 and 1.15. Similarly, for short walls, a variation of the normalised two-way bending capacity between 1.02 and 1.14 is observed. Regardless of the wall aspect ratio, walls with an opening located on the bottom corner show the lowest capacity, while walls with an opening centrally place show the highest capacity.

6.3.3. Influence of opening position on crack pattern

The influences of the opening position on the crack patterns of the long walls and short walls are presented in Fig. 30 and Fig. 31, respectively. In the grey-dot-lined boxes of each figure, the crack patterns of each case at the two-way bending capacity are shown to the left, and those at the end of the analysis are shown to the right to provide a reference on the further development of the crack patterns. Unlike the opening size and shape, the opening position can modify the crack pattern to some degree. For the long walls, when the opening is located at the bottom or top corner (L-WIN-PT11 or L-WIN-PT31), a major diagonal crack that should appear in its corresponding solid wall is missing, and the two-way bending capacity is the lowest. If the opening is located at the central left part (L-WIN-PT21), the diagonal crack above the opening originates from the opening corner rather than the wall corner, and multiple secondary diagonal cracks develop above and under the opening. In the case where the opening is located at the centre (L-WIN-PT22) or central top (L-WIN-PT32) of the wall, the positions of the major diagonal cracks are the same, and the central horizontal crack is missing in both cases. If the opening is located at the central bottom part (L-WIN-PT12), the horizontal crack occurs in the upper part of the wall, which together with the diagonal cracks contributes to the highest two-way bending capacity of all cases of L-WIN-SZ3. For the short walls, when the opening is located at the top (S-WIN-PT31), central top (S-WIN-PT32) and central left (S-WIN-PT21) part, the crack patterns are slightly affected except that multiple localised cracks develop from the wall corners. In the case where the opening is located at the bottom part (S-WIN-PT11), the diagonal crack shift to the top corner of the opening, and the bottom right diagonal crack elongates. If the opening is at the centre (S-WIN-PT22), the central vertical crack that should appear in the corresponding solid wall turns to be the horizontal crack above the opening. If the opening is at the central bottom part (S-WIN-PT12), the bottom diagonal cracks start from the wall corners, but develop upwards when they encounter the opening, and elongate diagonally again towards the wall centre.

7. Proposed equations and comparison with AS3700

In this section, fitting equations are proposed based on the influence of the opening on the two-way bending capacity studied in Section 6. The tendencies of these influences can be summarised as follows: i) the two-way bending capacity is exponentially related to the opening size (η), and this influence is interdependent on the wall aspect ratio (α) (Fig. 17); ii) the two-way bending capacity is positively correlated to the opening aspect ratio (α^*) (Fig. 25); iii) the vertical position of the opening (λ_x) has a very subtle influence on the two-way bending capacity; iv) the influence of the horizontal position (λ_y) of the opening is slight, but increases as the opening moves from the vertical edge towards the central line of the wall (Fig. 29); v) assuming the same opening size, aspect ratio and position, the difference between the two-way bending capacity of the walls with a window or door is small when the wall aspect ratio is small, but it increases to a large degree if the window is replaced with a door when the wall aspect ratio and opening size are large (Fig. 17). Based on these observations and applying nonlinear regression techniques, the proposed equations for the normalised two-way bending capacity are proposed as follows,

$$\frac{w_p}{w_s} = \beta_1 \cdot \exp(\beta_2 \eta \cdot \alpha^{\beta_3}) \cdot (\alpha^*)^{\beta_4} \cdot (\beta_5 |\lambda_x - 0.5| + \beta_6) + \beta_7 + \Delta \Delta = \begin{cases} 0 & (\text{for window}) \\ \beta_8 \cdot \eta^{\beta_9} \cdot \alpha^{\beta_{10}} & (\text{for door}) \end{cases}$$

$$\begin{cases} \beta_1 = 0.14; \beta_2 = 5.61; \beta_3 = -0.39; \beta_4 = 1.03; \beta_5 = -0.25; \\ \beta_6 = 0.14; \beta_7 = 1.00; \beta_8 = 1.74; \beta_9 = 3.10; \beta_{10} = 1.38 \end{cases} \quad (14)$$

where β_1 - β_{10} are constant coefficients; Δ is the supplement coefficient of the opening type. Here it is noted that the range of the opening

size (λ) is restricted between 0.2 and 0.8, which exclude cases of extremely small or large openings.

The comparisons of the proposed equations and the numerical results are presented in Fig. 32. Fig. 32a and b shows that the results of the proposed equations are very close to the numerical results when evaluating the influence of the opening type (door or window), size and wall aspect ratio. Fig. 32c, together with Fig. 25c, shows that the influence of the opening aspect ratio with varying opening size can also be well represented by the proposed equations. Fig. 32d shows that the proposed equations predict that the two-way bending capacity increases as the opening moves from the vertical edge to the central line, but is unrelated to the vertical position. The latter prediction is slightly different concerning the numerical results but is acceptable. The standard error of the regression is 0.07, which suggests the numerical results are quite close to the regression results. Overall, the proposed equations can evaluate the general tendency of the influence of the opening on the two-way bending capacity of the wall.

The proposed equations are further compared with Australian Standard – Masonry Structures AS3700 [25]. In AS3700, the opening area is considered non-covered and non-loaded. Even though AS3700 is more advanced compared to other codes and standards in terms of taking the influence of openings into account, it only considers the influence of the opening size (η) and horizontal position (λ_x). The influence of the wall aspect ratio (α) and the opening shape (α^*), which was found important to the two-way bending capacity of the perforated walls in this study, is not taken into account.

The comparison of the proposed equations and AS3700 is based on the experimental results of Wall 1 (solid wall) and Wall 3 (perforated wall) in Ref. [14]. Results are shown in Fig. 33. According to Fig. 33a, AS3700 predicts that the presence of an opening reduces the two-way bending capacity ($w_p/w_s < 1$) except a very few cases in which the opening is located in the wall centre and is either very small or large ($\eta < 0.2$ or $\eta > 0.8$). In contrast, the proposed equations suggest that the presence of an opening increases the two-way bending capacity ($w_p/w_s > 1$) for most cases. Besides, AS3700 predicts that the two-way bending capacity varies irregularly as the opening size increases (Fig. 33a), while the proposed equations predict that the former increases constantly as the increase of latter (Fig. 33b). Additionally, both formulas are in accordance that as the opening moves from the vertical edge towards the wall central line, the two-way bending capacity increases. These results reveal that large differences between AS3700 and the proposed equations exist regarding evaluating the influence of the opening on the two-way bending capacity of URM walls. Further physical experimental research is suggested to supplement more data for walls with various opening size, shape and position.

8. Conclusions

In this study, the influence of openings on the two-way bending capacity (defined as the peak pressure on the wall net area) of unreinforced masonry (URM) walls was investigated. First, a brief review was presented to reveal the major findings and limitations of the existing experimental campaigns on the comparable perforated and solid URM walls. Then, an evaluation of the arrangements of the openings (namely, the facts of whether the opening area is covered or non-covered, and whether it is loaded or non-loaded) by the Yield Line Method (YLM) was carried out. Next, numerical models were calibrated and validated based on selected experimental benchmarks and were further applied to study the influence of the arrangements of the opening area. Subsequently, a parametric study was carried out to evaluate the influence of the opening geometric parameters, namely, size, shape and position for walls with different aspect ratios. Eventually, analytical equations based on the numerical results were proposed and compared with the Australian Standard (AS3700). Conclusions can be drawn as follows:

- The existing experimental database concerning perforated URM walls in OOP two-way bending is limited in quantity. Even in each comparable testing group, the number of samples is quite small, so the high variability of material properties can affect the consistency of the results. Besides, the influence of opening size, shape and position has not been systematically studied by the experiments. Nevertheless, by comparing all the experimental results, the influence of the openings is found to be related to the arrangement of the opening area. The two-way bending capacity of a perforated wall is generally lower than that of its solid counterpart, provided that the opening area is covered and loaded as the rest of the wall; if the opening area is non-covered and non-loaded, the two-way bending capacity of a perforated wall can be higher than that of its corresponding solid wall.
- The YLM evaluation confirms that the arrangement of the opening area substantially influences the two-way bending capacity. This is in agreement with the experimental observations. However, it should be noted that relatively rough assumptions were made for this evaluation. For example, the moment capacity was assumed to be equal for both horizontal and diagonal cracks.
- Compared to the experimental benchmark, the 3D simplified brick-to-brick modelling predicts the two-way bending capacity to a quite reasonable extent, with a Mean Absolute Percentage Error of 11%. Besides, the numerical models precisely capture the crack patterns of the walls. Compared with the continuum modelling and the 3D detailed brick-to-brick modelling, the 3D simplified brick-to-brick modelling results as a good compromise to capture the response at the component level, in terms of wall capacity and crack pattern, with limited computational costs. The numerical results also confirm the experimental observations and evaluation of the YLM regarding the arrangement of the opening area.
- The parametric study indicates that when the opening area is non-covered and non-loaded, as the opening size (normalised as the ratio of the opening length to the wall length) increases, the normalised two-way bending capacity of the perforated wall (defined as the ratio of the capacity of the perforated wall to that of the solid wall) increases exponentially. With the same opening size, the two-way bending capacity of a wall with a door is higher than that of a wall with a window. This difference gets larger as the wall aspect ratio and opening size increase. Besides, at the two-way bending capacity, as the opening size increases, the deformation at the mid-height of the wall generally enlarges, and the crack pattern remains similar. Additionally, as the opening size increases, more cracks fully open per unit wall net area, which suggests more fracture energy is dissipated. This results in a higher two-way bending capacity.

- As the opening aspect ratio (the opening height to length) increases, the two-way bending capacity increases, the crack pattern remains similar. The influence of the opening position on the two-way bending capacity is limited. As the opening moves horizontally from the lateral edge towards the wall central line, the two-way bending capacity increases slightly. However, as the opening position varies, either vertically or horizontally on the wall, the diagonal cracks can shift positions, and more secondary diagonal cracks can appear.
- The proposed equations were proposed based on a close regression of the numerical results (standard error of the regression: 0.07). Compared with the proposed equations, AS3700 predicts that the presence of the opening weakens the wall capacity. Besides, AS3700 predicts that the two-way bending capacity varies irregularly as the opening size increases. Both the proposed equations and AS3700 predict a similar influence of the opening position on the two-way bending capacity. However, the influence of opening shape and wall aspect ratio on the perforated walls is not considered in AS3700 but can be predicted by the proposed equations.

In summary, systematically experimental study on the influence of openings on the two-way bending capacity of URM walls is scarce but necessary. Such study is beneficial for further development of the knowledge for the wall behaviour and can provide the basis for numerical study. Besides, the 3D simplified brick-to-brick modelling is suitable for simulating masonry at the structural component level, since it is computationally efficient and can capture the crack patterns precisely. Furthermore, the quantitative relations between the geometric parameters of openings and the two-way bending capacity of URM walls are acquired from the numerical study. These results are recommended to be incorporated for future updates of the analytical formulations.

Finally, it should be noted that the two-way bending capacity is defined in terms of pressure rather than force. This follows the conventions of current standards and is advantageous for comparing walls with various geometry. However, this definition can lead to irrational results for extremely large or extremely small opening sizes, which, however, are not common in practice. Therefore, the range of the opening size in the proposed equations is restricted according to practical scenarios.

CRedit authorship contribution statement

Lang-Zi Chang: Conceptualisation, Methodology, Software, Validation, Formal analysis, Investigation, Writing - original draft, review & editing, Visualization. Jan G. Rots: Writing - review & editing, Supervision. Rita Esposito: Conceptualisation, Methodology, Writing - review & editing, Supervision.

Declaration of competing interest

The authors declare that they have no known competing financial interests or personal relationships that could have appeared to influence the work reported in this paper.

Acknowledgement

The authors would like to express their gratitude to Dr Michael Griffith and Dr Jaroslav Vaculik for sharing the original experimental data. The financial support provided by the China Scholarship Council (CSC) to the first author is acknowledged. The first author would like to thank Miss Fortune and his friends from the Rift for their everlasting support and company.

References

- [1] E. Ahani, M.N. Mousavi, A. Ahani, M. Kheirollahi, The effects of amount and location of openings on lateral behavior of masonry infilled RC frames, *KSCE J. Civ. Eng.* 23 (2019) 2175–2187.
- [2] Z. Liu, A. Crewe, Effects of size and position of openings on in-plane capacity of unreinforced masonry walls, *Bull. Earthq. Eng.* 18 (2020) 4783–4812.
- [3] M. Yekrangnia, P.G. Asteris, Multi-strut macro-model for masonry infilled frames with openings, *J. Build. Eng.* 32 (2020).
- [4] D.F. D'Ayala, S. Paganoni, Assessment and analysis of damage in L'Aquila historic city centre after 6th April 2009, *Bull. Earthq. Eng.* 9 (2011) 81–104.
- [5] L. Moon, D. Dizhur, I. Senaldi, H. Derakhshan, M. Griffith, G. Magenes, et al., The demise of the URM building stock in christchurch during the 2010–2011 canterbury earthquake sequence, *Earthq. Spectra* 30 (2014) 253–276.
- [6] A. Penna, P. Morandi, M. Rota, C.F. Manzini, F. da Porto, G. Magenes, Performance of masonry buildings during the Emilia 2012 earthquake, *Bull. Earthq. Eng.* 12 (2014) 2255–2273.
- [7] L. Sorrentino, D. D'Ayala, G. de Felice, M.C. Griffith, S. Lagomarsino, G. Magenes, Review of out-of-plane seismic assessment techniques applied to existing masonry buildings, *Int. J. Architect. Herit.* (2016) 1–20.
- [8] D. Dizhur, J. Ingham, Seismic Improvement of Loadbearing Unreinforced Masonry Cavity Walls, Report - Branz ER3, New Zealand, 2015.
- [9] H.W.H. West, H.R. Hodgkinson, B.A. Haseltine, The resistance of brickwork to lateral loading, Part 1: experimental methods and results of tests on small specimens and full sized walls, *Struct. Eng.* 55 (1977) 411–421.
- [10] C. Southcombe, A. Tapp, Investigation of laterally loaded brickwork panels with openings, *Masonry* (2) (1988) 112–114, 1988, Stoke-on-Trent,.
- [11] V.L. Chong, The Behaviour of Laterally Loaded Masonry Panels with Opening [PhD Thesis], University of Plymouth, Plymouth, UK, 1993.
- [12] R.C. de Vekey, N.J. Bright, K.R. Luckin, S.K. Arora, The resistance of masonry to lateral loading, Part 3: research results on autoclaved aerated concrete blockwork, *Struct. Eng.* 64 (1986) 332–340.
- [13] B. Chen, Masonry Walls with Openings under Out-Of-Plane Loading (Master Thesis), McMaster University, Hamilton, Canada, 2002.
- [14] M.C. Griffith, J. Vaculik, Out-of-plane flexural strength of unreinforced clay brick masonry walls, *TMS Journal* 25 (2007) 53–68.
- [15] Ravenshorst GJP, F. Messali, C31B60: Out-Of-Plane Tests on Replicated Masonry Walls, Delft University of Technology, Delft, the Netherlands, 2016.
- [16] J. Vaculik, Unreinforced Masonry Walls Subjected to Out-Of-Plane Seismic Actions [PhD Thesis], University of Adelaide, Adelaide, Australia, 2012.
- [17] F. Graziotti, U. Tomassetti, S. Sharma, L. Grottoli, G. Magenes, Experimental response of URM single leaf and cavity walls in out-of-plane two-way bending generated by seismic excitation, *Construct. Build. Mater.* 195 (2019) 650–670.
- [18] J. Li, M.J. Masia, M.G. Stewart, S.J. Lawrence, Spatial variability and stochastic strength prediction of unreinforced masonry walls in vertical bending, *Eng. Struct.* 59 (2014) 787–797.
- [19] K.F. Abdulla, L.S. Cunningham, M. Gillie, Simulating masonry wall behaviour using a simplified micro-model approach, *Eng. Struct.* 151 (2017) 349–365.

- [20] A.M. D'Altri, S. de Miranda, G. Castellazzi, V. Sarhosis, A 3D detailed micro-model for the in-plane and out-of-plane numerical analysis of masonry panels, *Comput. Struct.* 206 (2018) 18–30.
- [21] A.C. Isfeld, M.G. Stewart, M.J. Masia, Stochastic Finite Element Model Assessing Length Effect for Unreinforced Masonry Walls Subjected to One-Way Vertical Bending under Out-Of-Plane Loading, *Engineering Structures*, 2021, p. 236.
- [22] L.-Z. Chang, J.G. Rots, R. Esposito, Influence of Aspect Ratio and Pre-compression on Force Capacity of Unreinforced Masonry Walls in Out-Of-Plane Two-Way Bending, *Engineering Structures*, 2021, p. 249.
- [23] E. Nasiri, Y. Liu, The out-of-plane behaviour of concrete masonry infills bounded by reinforced concrete frames, *Eng. Struct.* 184 (2019) 406–420.
- [24] European Committee for Standardization, Eurocode 6: Design of Masonry Structures, Part 1-1: General Rules for Reinforced and Unreinforced Masonry Structures, 2012. Brussels, Belgium.
- [25] Standards Australia, Australian standard for masonry structures (AS 3700:2018), in: , 2018. Sydney, Australia.
- [26] L.-Z. Chang, F. Messali, R. Esposito, Capacity of unreinforced masonry walls in out-of-plane two-way bending: a review of analytical formulations, *Structures* 28 (2020) 2431–2447.
- [27] H.W.H. West, H.R. Hodgkinson, B.A. Haseltine, R.C. de Vekey, The resistance of masonry to lateral loading, Part 2: research results on brickwork and aggregate blockwork since 1977, *Struct. Eng.* 64 (1986) 320–331.
- [28] B.A. Haseltine, J.N. Tutt, The resistance of masonry to lateral loading, Part 4: implications of research on design recommendations, *Struct. Eng.* 64 (1986) 341–350.
- [29] A. Tapp, An Investigate of Laterally Loaded Fenestrated Masonry Panels (Master Thesis), Polytechnic South West, Plymouth, UK, 1985.
- [30] R.C. de Vekey, G.J. Edgell, I.M. May, Lateral load behaviour of walls with openings, in: The 7th North American Masonry Conference, 1996. South Bend, US.
- [31] G.J. Edgell, E. Kjaer, Lateral Load Behaviour of Walls with Openings. 12th International Brick and Block Conference, 2000. Madrid, Spain.
- [32] C. Baker, B. Chen, R.G. Drysdale, Failure line method applied to walls with openings, in: 10th Canadian Masonry Symposium, 2005. Banff, Canada.
- [33] M.C. Griffith, J. Vaculik, N.T.K. Lam, J. Wilson, E. Lumantarna, Cyclic testing of unreinforced masonry walls in two-way bending, *Earthq. Eng. Struct. Dynam.* 36 (2007) 801–821.
- [34] B.A. Haseltine, H.W.H. West, J.N. Tutt, The resistance of brickwork to lateral loading, Part 2: design of walls to resist lateral loads, *Struct. Eng.* 55 (1977) 422–430.
- [35] British Standard, BS 5628-1 (2005): Code of Practice for the Use of Masonry, 2005.
- [36] S. Lawrence, R. Marshall, Virtual Work Design Method for Masonry Panels under Lateral Load. 12th International Brick/block Masonry Conference, Madrid, Spain, 2000.
- [37] P.K.V.R. Padalu, Y. Singh, S. Das, Analytical Modelling of Out-Of-Plane Flexural Response of Unreinforced and Strengthened Masonry Walls, *Engineering Structures*, 2020, p. 218.
- [38] L. Liberatore, O. AlShawa, On the application of the yield-line method to masonry infills subjected to combined in-plane and out-of-plane loads, *Structures* 32 (2021) 1287–1301.
- [39] D. Darwin, C.W. Dolan, A.H. Nilson, Design of Concrete Structures, McGraw-Hill Education, New York, NY, USA, 2016.
- [40] P.B. Lourenco, J.G. Rots, Multisurface interface model for the analysis of masonry structures, *J. Struct. Eng-Asce* 123 (1997) 660–668.
- [41] G.P.A.G. van Zijl, Computational Modelling of Masonry Creep and Shrinkage [PhD Thesis], Delft University of Technology, Delft, the Netherlands, 2000.
- [42] P.H. Feenstra, Numerical Simulation and Stability Analysis of Crack Dilatancy Models, TNO Building and Construction Research, Rijswijk, the Netherlands, 1989.
- [43] J.G. Rots, Computational Modeling of Concrete Fracture [PhD Thesis], Delft University of Technology, Delft, the Netherlands, 1988.
- [44] DIANA BV, DIANA User's Manual - Release 10.4, 2019. Delft, The Netherlands.
- [45] F. Karimi Ghaleh Jough, M. Golhashem, Assessment of out-of-plane behavior of non-structural masonry walls using FE simulations, *Bull. Earthq. Eng.* 18 (2020) 6405–6427.
- [46] S.J. Lawrence, Behavior of Brick Masonry Walls under Lateral Loading [PhD Thesis], University of New South Wales, Sydney, Australia, 1983.
- [47] A.M. D'Altri, V. Sarhosis, G. Milani, J. Rots, S. Cattari, S. Lagomarsino, et al., Modeling strategies for the computational analysis of unreinforced masonry structures: review and classification, *Arch. Comput. Methods Eng.* 27 (2019) 1153–1185.
- [48] S. Jafari, Material Characterisation of Existing Masonry: A Strategy to Determine Strength, Stiffness and Toughness Properties for Structural Analysis [PhD Thesis], Delft University of Technology, Delft, the Netherlands, 2021.
- [49] S. Jafari, J.G. Rots, R. Esposito, A correlation study to support material characterisation of typical Dutch masonry structures, *J. Build. Eng.* 45 (2022).
- [50] L. Liberatore, O. AlShawa, C. Marson, M. Pasca, L. Sorrentino, Out-of-plane Capacity Equations for Masonry Infill Walls Accounting for Openings and Boundary Conditions, *Engineering Structures*, 2020, p. 207.